Interpretation of high frequency climate signals in Antarctic ice cores

By
Wyatt Hansen
Geology, University of Colorado at Boulder

March 22nd, 2019

Thesis Advisors:
Dr. Tyler R. Jones, Institute of Arctic and Alpine Research
Dr. Gifford H. Miller, Geological Sciences

Defense Committee:
Dr. Gifford H. Miller, Geological Sciences
Dr. Mark Serreze, Geography
Dr. Leilani Arthurs, Geological Sciences

Table of Contents

ABSTRACT

Stable isotopes of hydrogen and oxygen in ice cores are useful for understanding hydrologic cycle processes, including local temperature, regional atmospheric circulation, and conditions at the moisture source. Spectral analysis of these isotopes, in terms of frequency content and the associated amplitudes, gives insight into the climate cycles that governed past climate changes. This study examines the West Antarctic Ice Sheet (WAIS) Divide ice core (WDC) and the South Pole ice core (SPC) using Multi-Taper Method (MTM) spectral analysis. The 3-7, 4-15, 15-30, and 30-50 year^{-1} bands are investigated in relation to past climate change. In prior studies, multi-year and decadal climate oscillations at WAIS Divide were linked to the topography of the Laurentide Ice Sheet (LIS) for the last 31 kyr. We extend this study, and find that for ages >31 ka, the signal strength drops, as expected from a smaller LIS at that time. There also appears to be no correspondence between the strength of the frequency bands and Antarctic Isotope Maxima (AIM) events. This suggests that AIM events are not related to fast paced (multi-year to decadal) climate signals. Analysis of deuterium excess (using the natural-log definition, dln) reveals a step-change in dln spectral power across all bands at ~13 ka. This may result from the Sunda Shelf (an extension of the continental shelf of Southeast Asia) flooding that changed convective properties and altered tropical Pacific-West Antarctic climate dynamics. Finally, we find a spike in spectral power across frequency bands in both WDC and SPC at ~20 ka. This time period is documented as the beginning of the deglaciation in West Antarctica. The spike in spectral power may be a representation of Critical Slowing Down, wherein the variance of the data increases just before a regime shift in the climate. These findings can be improved in future studies by including a robust diffusion correction for the multi-year frequencies, and Global Circulation Models could be used to elucidate regional and global climate connections.

Section 1.1. Introduction

Ice cores are cylinders of ice that have been drilled and extracted from ice sheets. An ice core contains layers of snow from the past, deposited during precipitation events, buried, and compacted into ice. The layers contain information about past climate, including trapped air bubbles, volcanic ash layers, and variable chemical compositions relating to atmospheric and oceanic circulation. In this study, we analyze water molecules with different molecular masses, which are known as isotopologues of water. In ice core science, the isotopologues of water can be used to reconstruct past temperature and regional atmospheric circulation, as well as infer changes in oceanic moisture source regions that provide snow to an ice core drilling site.

We utilize two ice core water isotope records: the West Antarctic Ice Sheet Divide ice core (WDC) and the South Pole ice core (SPC). These ice core records are well suited for analysis due to their high-resolution sampling. Mass spectroscopy has traditionally been used as the water isotope sampling technique. A newer technique, known as continuous flow analysis (CFA), is more time efficient and has higher data resolution (Jones et al, 2017). The sampling resolution allows for the analysis of annual, multi-year, and decadal variability in WDC and SPC across the last glacial-interglacial cycle. This can be done by looking at the amplitude of the signals in the ice relative to a given frequency. We can envision that our record is a combination of sine waves with certain frequencies and amplitudes. These frequencies represent different cyclical climate changes such as the dominant annual signal (1 yr^{-1}). By applying spectral analysis to the data, it is possible to analyze different frequency bands (e.g. 3-7 yr^{-1}) and their respective amplitudes (strength) through time. Changes in the strength of a frequency band may either represent diffusion in the upper layers of the ice sheet or climate change. Diffusion serves to reduce the amplitude of high-frequency signals in relation to the original climate signal.

Our goal is to analyze frequency bands within the range of 3-50 $year^{-1}$, quantify how the strength of these bands change through time, attempt to determine if diffusion plays a role, and ultimately offer insight into possible climatic causes of strength changes. Some research has already been done on high frequency signals in the WDC. This research spans the last 30 kyr and the results are discussed in two main papers: 1) a discussion of diffusion and its effects on the water isotope signal (Jones et al. 2017) and 2) climate interpretations of high frequency signals that are corrected for diffusion (Jones et al. 2018). This paper builds upon the studies by Jones et al. (2017, 2018) by analyzing further back in time (i.e. beyond 31 ka), performing spectral analysis on a wider range of frequency bands, and interpreting SPC in addition to WDC. In the remainder of the introduction, we explain water isotope chemistry in ice cores, the measurement techniques for water isotopes in ice, spectral analysis, and the interpretation of water isotopes for paleoclimate.

1.2. Water Stable Isotope Basics

1.2.1. The formation and uses of an ice core

The chemical composition of individual layers in an ice sheet is one of the main reasons paleoclimatologists know about the climate cycles of the last 740,000 years (Parrenin et al, 2007). Ice cores form from the deposition of many snowfall events. As snow continues to accumulate, the depth and pressure of individual layers increases and leads to the formation of ice. An isotopic analysis of this ice yields important paleoclimatic information such as temperature (Parrenin et al, 2007). The ice contains the isotopic composition of the snowfall event from which it formed and is governed by hydrologic processes (Gat, 1996). It is possible to deduce the characteristics of past climate change due to the extensive knowledge about how isotopes behave throughout the water cycle and how temperature plays a role in that process (Dansgaard, 1964).

1.2.2. Isotope definitions

Isotopes are versions of the same chemical element that have the same number of protons but different numbers of neutrons. In this study, we utilize some, but not all, of the isotopes of hydrogen and oxygen. The isotopes of hydrogen we use in this study include protium (1 proton, 0 neutrons; denoted as ^{1}H) and deuterium (1 proton, 1 neutron; denoted as D or ^{2}H). The isotopes of oxygen we use include ^{16}O (8 protons, 8 neutrons) and ^{18}O (8 protons, 10 neutrons). The mass difference between the different isotopes of oxygen and hydrogen are integral in isotope paleoclimatology. The abundance of these heavy isotopes in ice cores is a function of temperature (Dansgaard,1964). For this reason, ^{18}O and D are very useful tools for paleoclimatic reconstructions, they also can be used to trace the processes of the atmospheric water cycle (Dansgaard 1964, Dutsch et al. 2017).

Stable isotopes, such as D and ^{18}O, are useful tools for reconstructing the past because they do not decay with time and their abundance has been constant throughout Earth history. If a substance has its level of stable isotopes change throughout time it is due to changes in physical processes and not isotope abundance, therefore differences in the concentrations of these isotopes in a reservoir can be used to infer changes in varying physical processes. Out of the naturally occurring stable isotopes of oxygen, ^{16}O comprises 99.76% of the composition of oxygen, whereas ^{18}O makes up only 0.2% of the oxygen. Deuterium composes an even smaller proportion of hydrogen abundance and makes up 0.02% of the composition relative to the 99.98% protium makes up. Due to the rarity of ^{18}O and D, they are expressed relative to a standard and use per mil notation (‰). In equations 1 and 2, R_{sample} refers to the ratio between the concentrations of the heavy isotope to the most common light isotope (Galewsky et al. 2016). For example, R_{sample} can refer to the ratio between the concentrations of ^{18}O to ^{16}O (Eqn. 2). $R_{standard}$ refers to the heavy to light isotopic ratio of Vienna Standard Mean Ocean Water (Vienna Standard Mean Ocean Water). A typical value for $\delta^{18}O$ at WDC is -37‰.

$$\delta D = ((RD_{sample}/RD_{standard}) - 1)\ x\ 1000 \tag{1}$$

$$\delta^{18}O = ((R^{18}O_{sample}/R^{18}O_{standard}) - 1)\ x\ 1000 \tag{2}$$

Water is composed of hydrogen and oxygen; the varying molecular masses of this molecule are referred to as isotopologues. The most common isotopologue of water is $^1H_2{}^{16}O$. Isotopologues are molecules that have a set chemical composition but have varying masses due to the incorporation of different isotopes into the molecule. $^1HD^{16}O$ and $^1H_2{}^{18}O$ are other rarer isotopologues of water. During phase changes, isotopologues separate due to their differences in mass and bond strength; this process is called fractionation (Galewsky et al, 2016). Changes in the concentration of isotopologues in ice cores reflect changes in fractionation associated with the hydrologic cycle.

1.2.3. Fractionation

There are two main types of fractionation involved in ice core science: equilibrium fractionation and kinetic fractionation. Equilibrium fractionation is mass and temperature dependent (Kendall and McDonnell 1998). The mass of an isotope determines the bond energy of an isotope. Bond energy refers to how hard it is to break the bond of the isotope to a molecule which is a necessary process in chemical reactions. The heavier a molecule is, the higher the bond energy of the isotope and the harder it is to break the bond of the isotope. The differences in the bond strengths result in equilibrium fractionation with the harder to break bond becoming concentrated in the system where the molecules are bound (Kendall and McDonnell 1998). Temperature determines the amount of energy in a system and thus the amount of equilibrium fractionation that occurs. When it is hotter, a system has more energy and the differences in bond energy becomes minimalized. When it is colder, such as at the poles, there is less energy in the system which results in there being larger equilibrium fractionation (Kendall and McDonnell 1998).

Equilibrium fractionation describes a process that is bidirectional. This means that a reaction is reversible, such as when vapor turns into condensate, but condensate can also turn into vapor. This is referred to as isotopic exchange and generally results in the heavier isotope becoming more concentrated in the denser and more stable material, i.e. in liquid water rather than vapor (Gat, 2002). Due to the bidirectionality of equilibrium fractionation, the product or reactant can become enriched in the heavy isotope (Kendall and McDonnell, 1998). In the phase change example of condensation, ^{18}O and D become more concentrated in the condensate while ^{16}O and ^1H become more concentrated in the vapor. Equilibrium exchange fractionation is explained in equation 3 where R represents the ratio between the heavy and light isotope, A and B are the two substances involved in the reaction, and α is the fractionation factor (Kendall and McDonnell 1998)

$$\alpha_{A\text{-}B}=R_A/R_B \tag{3}$$

Kinetic fractionation is a type of fractionation that happens when a process is unidirectional. Kinetic fractionation occurs due to the differences in the rate of reaction of isotopes based on mass and velocity. At a given temperature, the kinetic energy of a system is the same for all isotopes. Kinetic energy is based on the velocity and mass of a molecule (Eqn. 4). When kinetic energy is the same between two molecules, the heavier molecule will have a slower velocity. This process typically results in the reactants having a greater concentration of the heavy isotopes relative to the products. (Dansgaard, 1964). The differences in chemical reaction rates between different bonds will lead to kinetic fractionation if the process happens outside of equilibrium, this is a kinetic isotope effect (Melander 1960). Kinetic fractionation usually has a greater fractionation than equilibrium fractionation (Kendall and McDonnell 1998).

$$KE = 1/2(mv^2) \tag{4}$$

1.2.4. Isotopes in the water cycle

Water cycle processes discriminate against certain isotopes which leads to fractionation. Evaporation, condensation, and precipitation all effect the ratio of the heavy isotopes relative to the light isotopes in different reservoirs. In order to make conclusions about paleoclimate, it is necessary to fully understand these processes and the degree of fractionation involved in them.

Despite the first site of evaporation happening up to thousands of miles from the snow in Antarctica, evaporation is a fundamental process in ice core science. In addition to equilibrium fractionation, kinetic evaporation occurs when there is not enough time for liquid water and vapor to reach equilibrium. During kinetic fractionation, wind prevents equilibrium conditions at the ocean-atmosphere interface. This is because the resulting water vapor from evaporation is transported out of the system by wind. This process leads to a greater ratio of the ^{18}O and D relative to ^{16}O and ^{1}H in ocean water compared to the evaporated water (Gat, J.R, 2003). The water isotopic composition in a parcel of air formed through evaporation is determined by the original isotopic composition of the ocean source, the isotopic composition of the vapor already in the atmosphere, the relative humidity, the equilibrium fractionation factor, and the kinetic fractionation reflective of the differential rates of reaction among isotopologues (Galewsky et al, 2016). In the case that evaporation proceeds slow enough such that equilibrium conditions can be met, then the fractionation factor is solely the ratio between the vapour pressure of the light component (p) and the heavy component (p') seen in equation 5 (Dansgaard, 1964).

$$\alpha = p/p' \tag{5}$$

In contrast to evaporation, condensation is an equilibrium process that has varying fractionation amounts. In a cloud, the heavy isotopes prefer the denser phase (liquid) than the less dense phase (vapor). As a moisture mass moves poleward, the $\delta^{18}O$ and δD values will become more negative through subsequent condensation and the removal of the heavy isotopes.

1.2.5. Rayleigh distillation

Rayleigh distillation explains the isotopic effects of poleward moving clouds. When an air parcel (i.e. a cloud) becomes colder at higher latitudes, the isotopic composition of the cloud changes after each rain or snow event. In a generalized view, cloud formation occurs in the tropics where evaporation dominates. Here, the isotopic value of ocean water is assumed to be 0‰ (VSMOW), and water vapor that evaporates from the ocean has a $\delta^{18}O$ value of about -12‰. This evaporation contributes to the formation of clouds. Upon condensation, the first rainout will be about -1‰, roughly 11‰ heavier in $\delta^{18}O$ than the remaining vapor. Subsequent condensation events will lead to isotopically lighter vapor in the cloud, thus the future rainout is also isotopically lighter. In Figure 1, ε represents the fractionation between water vapor and condensate. As the residual vapor fraction decreases in an air parcel, the fractionation increases. When the cloud reaches polar regions, the condensate transitions from rain to snow. This change of condensate is important because there is a greater fractionation between water vapor and snow than water vapor and rain. Vapor to snow has an ε of 14.7‰. The isotopic composition of the condensate can be found with equation 6 (Galewsky et al, 2016). The isotopic content is a function of the temperature gradient the cloud experienced on its poleward trajectory. Therefore, the isotopic composition of ice in the poles can be used to trace temperature histories through time as it relates to the hydrologic cycle. This is the basis for ice core science and paleothermometry.

$$R_r = R_o f^{\alpha_v{}^{l}(T)-1} \tag{6}$$

where R_r is the isotopic ratio of the vapour, $R_o$is the initial composition of the vapour, f is the fraction of the original vapour remaining, and $\alpha_v{}^{l}(T)$is the temperature dependent fractionation factor between phases.

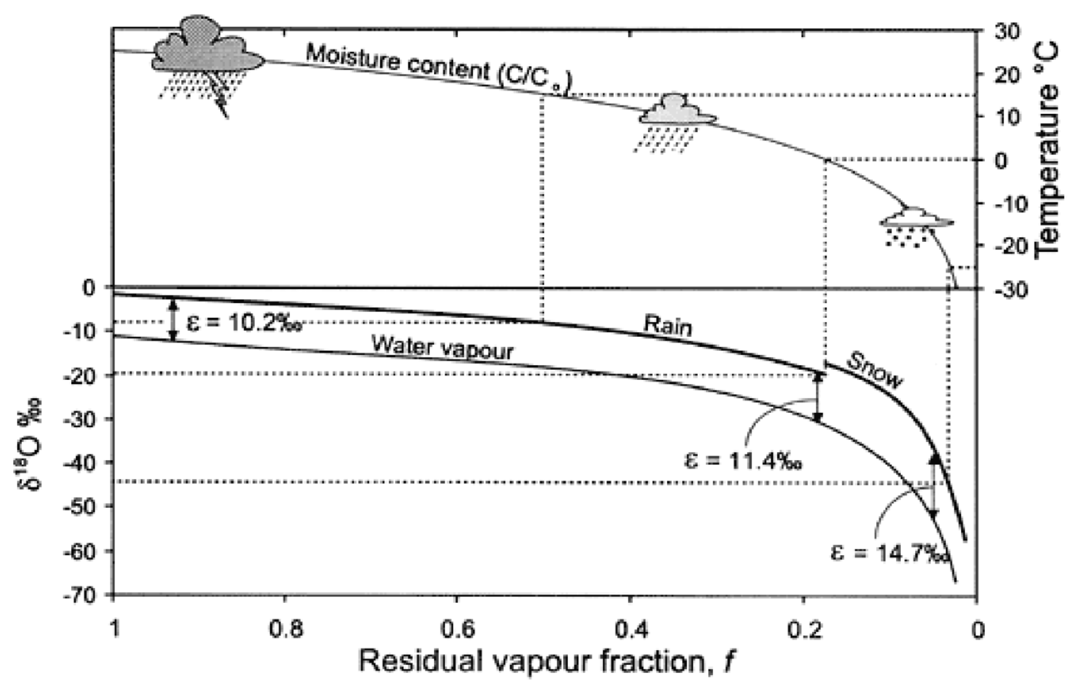

Figure 1 (Clark and Fritz, 1997): Fractionation as a function of water phase and temperature.

After conducting a worldwide survey, Harmon Craig found an equation (Eqn. 7) that demonstrated the relationship between the two isotopes at equilibrium (Craig, 1965). The equation reflects the values of δD and δ^{18}O in meteoric waters and precipitation. When δ^{18}O and δD are plotted against each other globally, a straight line is formed with a slope of 8. This line is known as the Global Meteoric Water Line (GMWL) (Figure 2). Plotting δD against δ^{18}O also allows for investigating processes in which the two heavy isotopes interact differently with the environment causing a slope different than the GMWL (Dansgaard, 1964). Deviations from this line usually represent kinetic effects such as humidity (Gat, 1996). Because the intensity of kinetic effects depends on temperature, mass differences, humidity, and molecular diffusivities, deviations can be powerful paleoclimatic tools (Jones, 2010).

$$\boldsymbol{\delta}D=8(\boldsymbol{\delta}^{18}O)+10 \quad \textbf{(7)}$$

$$d=\delta D-8\cdot\delta^{18}O \quad \textbf{(8)}$$

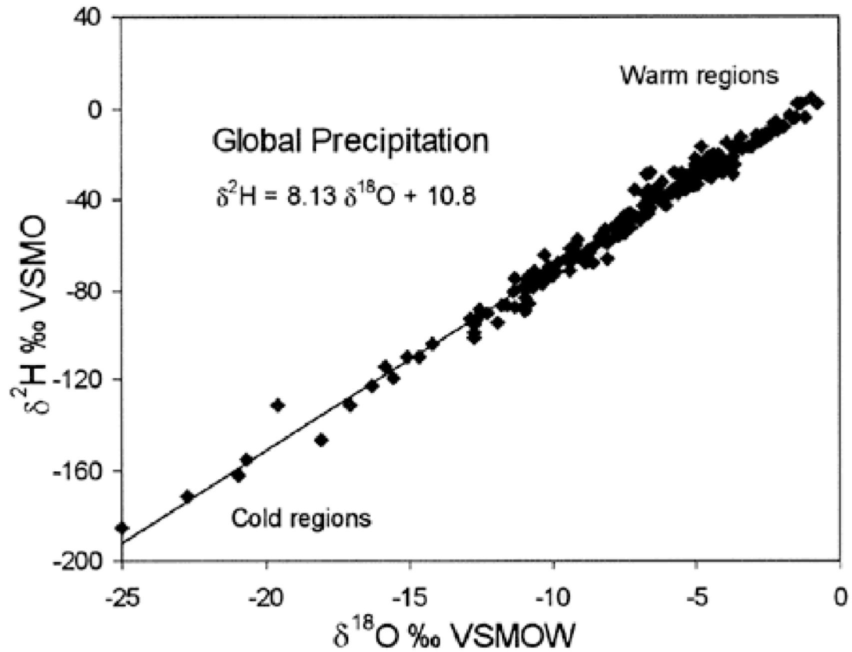

Figure 2 (Clark and Fitz, 1997): Global Meteoric Water Line

1.2.6. Deuterium excess

Deuterium excess is a second order parameter that is used to describe the deviations from the GMWL (Dansgaard, 1964). Due to differences in reaction rates based on mass, deuterium is much less sensitive to kinetic effects than ^{18}O (Dansgaard, 1964). This leads to a surplus of deuterium relative to the GMWL, the surplus is known as deuterium excess (dxs) (show by Eqn. 8). The dxs is used to understand the impact of kinetic effects on water isotopes and to interpret paleoclimatic conditions. Although dxs is thought to primarily relate to moisture source conditions (i.e. oceanic conditions at the location of the evaporated water that eventually falls as snow at an ice core site), the factors that control it are argued (Pfahl and Sodemann 2014, Steen-Larsen et al. 2014).

A classic interpretation of dxs is that it is a function of relative humidity, wind speed, and sea surface temperatures at the evaporation site (Merlivat and Jouzel, 1979). Other than changes in the parameters above, changes in dxs can be interpreted as changes in the location of the evaporation source as a result of a reorganization of atmospheric circulation (Dutsch et al, 2017). In a study done by Benetti et al. (2014) of ocean conditions at 26°N, it was found that relative humidity was inversely correlated to dxs. A 25% increase in relative humidity at the sea surface resulted in a 10‰ decrease in dxs. The same study found that a variable and stronger wind regime resulted in 5‰ variation in dxs values compared with a smooth wind regime. This is because high winds speeds lead to turbulent diffusion at the ocean-atmosphere interface, which increases fractionation (Benetti et al. 2014). However, the study found that sea surface temperatures (SST) had a negligible effect on dxs. Pfahl and Sodemann (2014) had similar findings and assert that relative humidity is the main control on dxs while SST only appears to effect dxs due to the relationship it has with relative humidity. Pfahl and Sodemann's findings are based off of observations of dxs on daily timescales that showed a much higher correlation of relative humidity and dxs than SSTs. Conversely, in a 2013 study of ice core sites in both Greenland and Antarctica, Lewis et al. (2013) found that dxs does trace source SST, but relative humidity and wind speed are also important factors. If SST does not relate to dxs, some paleoclimate interpretations may need to be re-examined.

It was previously thought that an ice core's isotopic composition was solely the result of the isotopic composition of precipitation that fell on the ice sheet. However, post deposition events (rather than just moisture source conditions) have been shown to impact dxs as well (Steen-Larson et. al, 2011). Newer research using laser spectroscopy instruments is showing that the ice sheet is in constant communication with 6-20% of the snow surface mass exchanging with the near surface water vapor in the atmosphere (Steen-Larson et al. 2013). The near surface water vapor changes as a result of atmospheric circulation changes. Changes in atmospheric circulation results in moisture from different sources and distillation paths changing the isotopic composition of the near surface atmospheric water vapor. In between precipitation events, the isotopic composition of the snow changes to reflect near equilibrium values with the near surface atmospheric water vapor (Steen-Larson et. al, 2011). This alteration of surface snow isotopic composition results in changes of dxs values. For example, the dxs of Greenland surface snow could become higher as moisture inflows from higher latitudes. The high-latitude Arctic has low temperatures and is dry, therefore air parcels from the Arctic have experienced strong kinetic fractionation leading to lighter water isotope compositions and a higher dxs value. Water tagging in atmospheric models have helped confirm this hypothesis (Steen Larson et al. 2014). This essentially means that water vapor in the atmosphere is affecting the ice sheet's isotopic composition, including dxs. The dxs values can also change through the process of wind scouring. Katabatic winds can transport snow from one place to another on the ice sheet. For example, the isotopic composition of inland, high elevation snow is usually more negative than the snow in lower, less inland locations. Through wind scouring the isotopic signal of snow can be mixed with different snow which will also change the dxs values. Diurnal snow metamorphism can also affect the dxs values (Casado et al. 2016). During summer there is a large temperature differential between night and day in Antarctica. At night, snow is added to the ice sheet through condensation and during the day snow is lost through sublimation. Due to the temperature effect on fractionation, there is a net increase in heavy isotopes in the snow as more heavy water isotopes are added at night than lost during the day (Casado et al, 2018). Grain size index of snow can be used to interpret how much sublimation has occurred with more sublimation resulting in larger grain sizes. These ideas are actively being researched and how the processes affected dxs are still debated.

Any interpretation of dxs (or its natural log definition, dln; see below) must be made with this uncertainty in mind.

1.2.7. The natural log of deuterium excess, dln

Due to supersaturation effects in the atmosphere, dxs is not properly defined when considering water isotopes at very high latitudes. To account for this problem, the natural log of deuterium excess (dln) is used (Eqn. 8) (Schoenemann et al. 2014). The dln captures differential temperature sensitivities of equilibrium fractionation for δD and δ^{18}O better than dxs (Schoenemann et al. 2014). It should be used for high-latitude ice cores sites, including WDC and SPC.

$$d_{ln} = ln(\delta D + 1) - (-2.85 * 10^{-2}(\ln(\delta^{18}O + 1))^2 + 8.47(\ln(\delta^{18}O + 1)) \quad \textbf{(8)}$$

1.2.8. Diffusion

Diffusion occurs at the top of an ice sheet inside the firn, within solid ice, and at the base of the ice (Jones et al. 2017). Firn diffusion modeling allows for the impact of diffusion to be minimalized in analysis, solid ice molecular diffusion has a smaller impact on the isotopic composition of a signal and geothermal diffusion impacts the deepest ice which prevents analysis of the oldest ice in a core (Jones et al. 2017). Diffusion alters the isotopic signatures of individual bands by blending together different isotopic compositions. If the isotopic composition of a winter and summer are blended together then the isotopic signature of that ice will show a much more averaged signal than the temperature fluctuations expected between summer and winter. A lower amplitude 1 year^{-1} could signify that there was little temperature change between winter and summer or that diffusion has smoothed out the annual isotopic values. If diffusion can be corrected for, it will be possible to better understand long term and abrupt climate change. See 3.3.3 for further information on diffusion.

1.3. Climate Cycles and Ice Cores

Climate variability is the expression of many physical processes operating concurrently. These cycles range from daily to millennial scales (or longer) and can amplify or diminish the effects of other climate cycles depending on how they align with each other. Ice cores record this variability through changes in the isotopic composition of the ice through time. Ice cores in Antarctica have been used to show Milankovitch cycles (100 to 10s of thousand year cycles) (Watanabe et al. 2003), Antarctic Isotope

Maxima events (multi-thousand year cycles) (Markle et al. 2017), all the way to decadal and multi-year cycles (Jones et al. 2018). In this study, we focus on patterns observed at multi-year to decadal timescales.

1.3.1. Milankovitch cycles

The current geologic period (Quaternary), is marked by cyclical global climate change. During this time the Earth has experienced many glacial-interglacial cycles, resulting in the growth and reduction of ice sheets and associated changing sea levels. During these cycles the Earth's global temperature fluctuated dramatically. Evidence of these changes are seen through the oscillating values of δ^{18}O using benthic foraminifera and ice cores. When these δ^{18}O values are plotted against time a repeating pattern appears. The wavelength of these cycles correlates to orbital variability.

Earth's orbital orientation and movement can be described by precession (wobbling of axis), obliquity (tilt), and eccentricity (circularness of orbit) (Figure 3). Each characteristic directly impacts the solar energy distribution across Earth's surface through time. A sufficient reduction of solar energy distribution at 65 degrees North during summers can allow ice sheets to grow, as long as winter snows do not completely melt in the summer months.

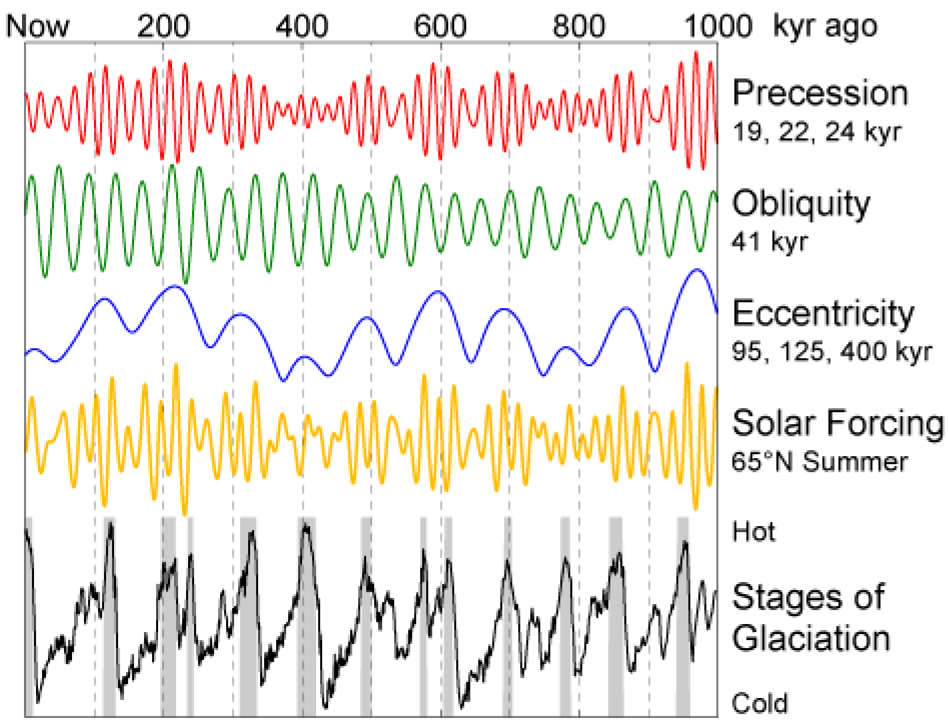

Figure 3: Milankovitch cycles, solar forcing, and stages of glaciation (Generalic, 2019).

Precision refers to the orientation of the Earth's axis as it wobbles; this cycle is 23,000 years long. Currently the precession of the Earth cause Polaris to be the north star, the other end of the cycle has Vega as the north star. During certain parts of the precession cycle, the Northern Hemisphere will experience summer during perihelion, when the Earth is closest to the sun. Obliquity is the axial tilt of the Earth; this cycle is 41,000 years long. The Earth does not spin vertical on its axis, instead it is tilted at an angle from 21.5 to 24.5 degrees from horizontal. Tilt creates seasons by varying the amount of solar flux an area receives throughout the year. This variability increases with increased latitudes. The larger the tilt, the greater the seasonality of an area. Seasonality is the difference between summer and winter solar flux. A larger tilt results in greater summer insolation which means the poles are receiving more solar energy during the summer and can melt more ice. A smaller tilt results in less summer insolation and the growth of ice sheets. Eccentricity refers to the circularness of Earth's orbit, with oscillations of about 100 to 125 thousand years, and a larger cycle of 400 thousand years. Eccentricity modulates the impact of precision. If the orbit is completely circular then precision does not change the climate of the Earth. If the orbit is eccentric then precision will determine which hemisphere receives the highest insolation during the perihelion. Eccentricity has been suggested as a factor in glacial-interglacial cycles, and appears to govern the last 8 glacial cycles seen in ice cores, but the reason is not exactly clear (Lisiecki, 2010).

1.3.2. D-O events

In-depth analysis of Greenland's ice cores has found that abrupt warming events occured in the last glacial period. The warming of these events could reach as high as 10 degrees Celsius in Greenland (Schulz 2002). These events are called Dansgaard Oeschger events (D-O events), which refer to abrupt warmings that occurred within years to decades. About 25 of these events occurred during the last glacial period (Rasmussen et al, 2016), separated in time by about 1-5 thousand years. Many mechanisms have been proposed for the D-O events. Labeyrie et al. (2013) noted that every D-O cycle correlate to a large-scale change in the organization of atmospheric circulation in the North Atlantic. One of the most accepted hypotheses is that D-O events are the result of a change in the circulation of the Atlantic Meridional Overturning Cycle (AMOC) (Rasmussen et al. 2016). Currently the AMOC system delivers warm water to Greenland and the North Atlantic. If AMOC stopped or slowed down, the result would be partial thermal isolation of the North Atlantic, leading to a decrease in temperatures of Greenland. It is estimated that AMOC would stop if 0.1 Sv (1,000,000 cubic meters of water/second = 1 Sv) of freshwater entered the North Atlantic (Labeyrie et al. 2013). This process could also be caused by 1 Sv of freshwater entering over 100 years. Similarly, if AMOC resumed, it could lead to abrupt warming.

If AMOC stopped or slowed in the glacial due to freshwater input, this could result in up to a 15 degree temperature drop and the creation of a stadial cold period (Labeyrie et al. 2013). Heinrich events may have been what caused the increase in freshwater in the North Atlantic. Heinrich events are seen by an increase in IRD (ice rafted debris) in ocean sediment cores. An increase in IRDs is a signal for increased ice sheet growth that caused an eventual purging of icebergs (and freshwater) into the North Atlantic. This could interfere with thermosaline density of the North Atlantic Deep Water (NADW). However, there is no evidence that there is a Heinrich event that corresponds with every D-O event, thus other processes are likely at play.

Glacial stadials in Greenland (in-between D-O warming events) coincide with gradual warming in Antarctica. This is caused when AMOC is weakened or stopped, causing warm water that once moved North from the tropics to the North Atlantic to instead accumulate in the Southern Hemisphere. The back and forth movement of ocean currents associated with AMOC throughout the glacial period was dubbed the "bipolar seesaw" (Broecker,1998). At the onset of an abrupt warming event in Greenland, Antarctica begins to cool about ~250 years later (WAIS Project Divide Members, 2015). There is a one to one correlation between D-O events and Antarctic Isotope Maxima events (AIM) in Antarctica (Labeyrie et al. 2013). AIM events have a more gradual warming and cooling than D-O events and a smaller amplitude. During D-O events, Greenland dxs is antiphased with $\delta^{18}O$ and δD (WAIS Project Divide Members, 2015). This means that as dxs increases, $\delta^{18}O$ and δD decrease. This could be a result of changes in the conditions of the moisture source or changes in the moisture source during D-O events.

1.3.3. Decadal and interannual climate cycles

In addition to Milankovitch forcing and D-O/AIM events, climate cycles exist at many other frequencies. Recent advances in ice core science have allowed for the interpretation of climate at the highest-frequencies yet possible: annual, multi-year, and decadal time scales. Note that centennial cycles are also a topic of study, but the literature is limited, and we do not include an analysis here. El Nino Southern Oscillation (ENSO) is a well-known multi-year climate cycle affecting the tropical Pacific. In modern times, ENSO has a periodicity of 2-7 years. Different responses to ENSO are seen through patterns of trade winds, ocean currents, precipitation, and SST (Mcphaden et al. 2006).

A study done by Jones et al. (2018) illuminated the importance of the 4 to 15 year^{-1} frequency band in Antarctica. The study examined changes in the strength of the 4 to 15 year^{-1} frequency band at WDC. The frequency band was found to be stronger during 16-31 ka than from the present to 16 ka. At 16 ka there was a large decline in the strength of the frequency band. The changes in the strength of the frequency band was hypothesized to represent changes in a teleconnection between the Laurentide ice sheet, the tropical Pacific, and Western Antarctica. A teleconnection describes a relationship between two or more distant regions of Earth where a change in one region results in a change in the other. This process is often perpetrated by changes in atmospheric and oceanic circulation. The size of the Laurentide ice sheet was the deterministic factor for how the teleconnection functioned (Jones et al. 2018). During the glacial period, when the Laurentide was largest (Ullman et al. 2014), the topography of the ice sheet was able to shift atmospheric circulation patterns. The shifted atmospheric circulation was felt in the tropical Pacific through altered Rossby waves which lead to increased atmospheric anomalies near Antarctica. The atmospheric anomalies created a more variable multi-year to decadal climate in Antarctica which is seen through the high power density values of the 4 to 15 year^{-1} frequency band. The drop in power density values at 16 ka reflect a regime shift in the teleconnection representing a weakened ocean-atmosphere coupled state. Heinrich event 1 occurred at 16 ka which was seen by a large discharge of icebergs into the North Atlantic from the Laurentide ice sheet. Heinrich event 1 signified a decrease in the topography of the Laurentide ice sheet past a critical point where the ice sheet could no longer effectively alter atmospheric circulation. Without the topography, the atmospheric anomalies that were affecting Antarctica disappeared and the variability of the multi-year to decadal climate decreased resulting in the drop in the strength of the 4 to 15 year^{-1} frequency band.

1.4. Objectives

The purpose of this study is to analyze how stable isotopes and high frequency signals have changed through time. This will be accomplished using spectral analysis on the water isotope data. This study will investigate variations in high frequency signals and find how they correlate to D-O and AIM events. This study also aims to find robust signatures of climate change that occur across multiple frequency bands and within separate ice cores. To aid in analysis of the high frequency data, a preliminary diffusion assessment will be performed to assess the approximate role of diffusion in the frequency signals.

Section 2: Methods

2.1. Accumulation Rates and Dating

In order to use isotopic compositions of ice for spectral analysis and to identify climatic cycles, it is necessary to be able to determine accumulation rates and date the age of the ice. Accumulation of snow in the WDC record is much higher than ice core sites from East Antarctica, including SPC. The WDC ice core team found the accumulation rate of ice using assumptions such as a temporally constant firn density profile, constant ice thickness, and a basal melting rate of a centimeter per year (WAIS Divide Project Members, 2013). The timescale of the WDC record was done using high resolution chemical measurements and electrical conductivity.

Even though high accumulation rates make counting annual layers easier, a multi proxy approach was taken for dating the most recent 31.2 ka ice. Electrical conductivity of ice changes throughout the year, electrical conductivity analysis tracks this change and employs it as a way to measure annual layers (Sigl et al. 2016). Three different types of electrical analysis were used, dielectric profiling (DEP), as well as alternating and direct electrical conductivity measurement (AC-ECM) (DC-ECM) (Sigl et al. 2016). DEP was essential for dating the brittle section of ice between 577-1300 meters because it still functions in the fracture zones that make up the brittle ice.

Chemical changes within the ice served as other proxies for tracking annual layers. One chemical proxy used was black carbon which follows yearly cycles. Black carbon forms as a result of wildfires and burning of fossil fuels (Sigl et al. 2016). In the Antarctic record, there is an annual maximum of black carbon in autumn corresponding to the largest wildfire season of the southern hemisphere. Sea salt is present in the ice core record and is governed by a seasonal cycle as well. Sea salt has a maximum in winter due to the ocean being rougher and stormier in winter creating more sea spray and thus more sea salt deposition. Aerosols are deposited differently throughout the year due to fluctuations in source strength and the changes in transport efficiency and are used for dating as well. A problem with using annual chemical cycles for dating the record is that if the parameter had a weak signal one year it is possible that the layer was not counted as a year. Beryllium 10 (^{10}Be) in the ice was compared to carbon 14 (^{14}C) in tree ring records. Both are radionuclides and therefore respond to changes in cosmic rays, this relationship is useful back to 12 ka, where tree ring records stop, but the resolution of the record is only 10-30 years (Muscheler et al. 2014).

The multiple proxy approach makes WDC unique among Antarctic ice cores, however individual layer counting was also utilized. Individual layer counting was done manually, using a straticounter algorithm, and a selection curve system (Sigl et al. 2016). These systems worked together to check the accuracy of measurements done by the other systems by comparing results. Both the selection curve and straticounter system work well with large uniform annual layers but have a hard time interpreting smaller and more variable layers where manual interpretations are the most convenient.

Historical events are another useful parameter for dating ice cores. One example is the 150 year long acid deposition event that is present within the record. This event caused by volcanoes is present in other records and can be used to correlate the age of the record to other records. Volcanic ash layers function in the same way.

In the top 2850 meters of the ice core, the uncertainty of the timescale is remarkably small. The uncertainty of each section is determined by comparing the total age of each section found by a measurement technique compared to other measurement techniques. An example of this is the section of 1940 to 2020 meters. In this section, the WAIS Divide Project Members compared the aerosol/ECM ages determined in 2006 with the ages determined by the straticounter interpretation of the parameters. The comparison found an age difference of 16 years between interpretations which resulted in a 2 percent uncertainty (Sigl et al. 2016). Another approach to dating the record is to correlate the record to other high-resolution records. The Intcal13 carbon tree ring record was found to be only 10 years older than the ^{10}Be record of the ice core at 11 ka (Sigl et al. 2016). Comparisons were also made to the NGRIP ice core and Hulu cave speleothem record.

The record after 2850 meters is not dated with annual cycles due to the amplitude of the cycles decreasing to an unreadable point. Other ice cores have used orbital tuning or ice flow models to date the cores. The age of the WDC reaches 68 ka which encompasses only 3 precession changes and thus is not useful or high enough resolution for this core (Buizert et al. 2015). There are too many uncertainties with accumulation, ice flow and ice sheet elevation to use the ice flow model. The WDC deep ice core was instead dated using methane synchronization techniques (Buizert et al. 2015).

The methane in WDC was compared to the δ^{18}O in NGRIP ice core and the Hulu cave Speleothems. Both records are high resolution and have been dated using other techniques such as U/Th for the speleothems (Buizert et al.2015). Therefore, if WDC is matched to locations of the other two records the age can be known. Inside each record is methane. This gas is useful because it is globally well mixed and has a varying signature through time (Buizert et al. 2015). The main problem with the methane inside WDC is that methane bubbles are not necessarily in situ with ice that formed at the same time, this is known as the Δage. While in the firn, the uppermost layer of the ice sheet, the air bubbles can interact with the atmosphere which makes them younger than the ice they are in (Schwander and Stauffer, 1984). To deal with this problem, a coupled firn-densification-heat-diffusion model was created. This is used as an inverse model in which the δ^{15}N is used to find the Δage. The Δage allows for the age of the ice to be found after the age of the methane has been found through correlating its signature to the other records.

Once the methane has been found it is connected to the δ^{18}O of the NGRIP and Hulu records. Both methane and δ^{18}O change during D-O events, the first step in the correlation process is to identify D-O events and find the midpoint of each in the methane and δ^{18}O records. After this is done a gas age can be applied to the methane based off of the age of the δ^{18}O of the other records. Then using the Δage found using the model, an age depth relationship can be found. Afterwards the age is interpreted until the next D-O midpoint.

SPC was drilled after WDC and does not contain published papers about the accumulation rate and timescale. The SPC has an annual resolution for 11,341 years. Research is still being done on SPC accumulation and the timescale is actively being worked on (University of Washington).

Figure 4: CFA System

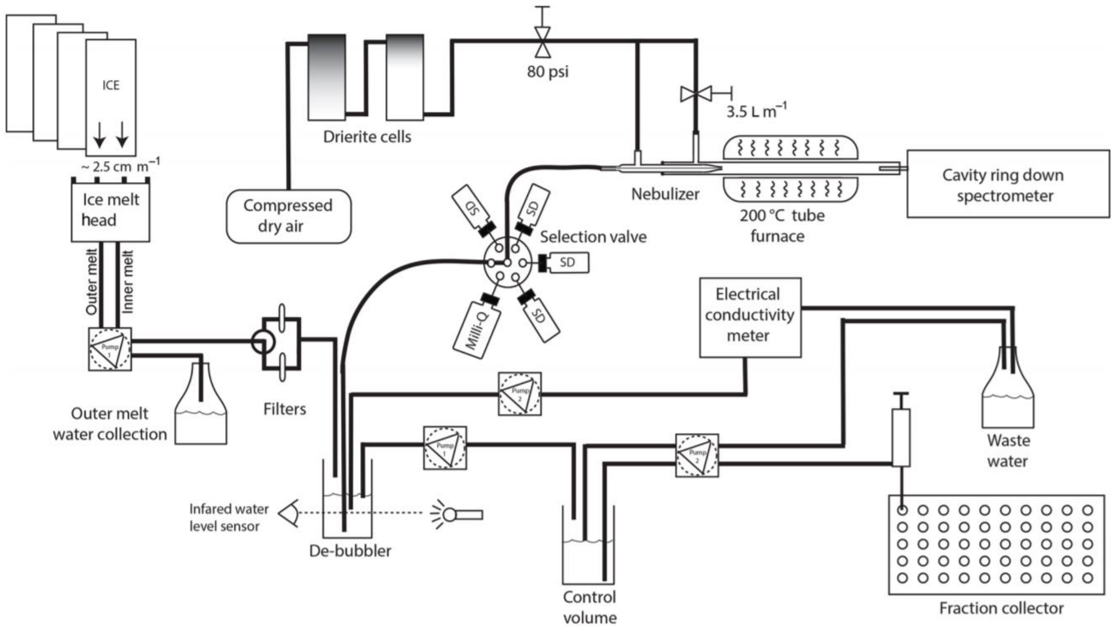

2.2. CRDS-CFA System

The information utilized in this study was obtained using a cavity ring down laser spectroscopy (CRDS) system coupled to a continuous flow analysis (CFA) (Jones et al. 2017). Previous sampling techniques of ice cores, namely mass spectroscopy, were time consuming and had a much lower resolution for the time put into analysis. The CRDS-CFA system (Figure 4) melts the ice, converts the liquid to gas, and then analyzes the isotopic composition of the water vapor (Jones et al. 2017). The melting component of the system consists of a rotating carousel, an aluminum heating block, a temperature controlled bath, a melthead, and a laser. The carousel rotates the ice immediately after the melting of one ice stick. This ensures that the analysis is in fact continuous. Depth-registration is accomplished by communicating with a laser that tracks the distance between the ice and the melthead. Once melted, the water from the inner catchment area is pumped away and filtered. A primary flow tube collects a fraction of the water for analysis; the rest of the water is used for other purposes. Liquid water is then pushed through a nebulizer supplied with high pressure dry air, converting the water into a fine spray. After the nebulizer , the spray is subjected to heating of 200 degrees Celsius inside a furnace. The water vapor concentration for the system is maintained at around 25,000 ppm H_2O, the optimal range for the laser. Once converted to a vapor, the water enters a Picarro L2130-i analyzer, where it is measured for isotopic composition using Laser pulses and mirrors (Crosson, 2008).

2.3. Spectral Analysis

Once all the data has been collected using the CRDS-CFA system and the age of the ice has been found, it is possible to use the data for interpreting climatic cycles. The data is a combination of waves at different frequencies, acting together to make the signal we see. In a water isotope record in ice cores, these frequencies are visible by taking data in the time domain and placing it in the frequency domain using a fast fourier transform (FFT) or other spectral analysis techniques. FFTs find the amplitudes of the frequencies that make up the signal. Essentially, the FFT reconstructs the signal using sine and cosine waves, each with their own unique wavelength and amplitude. FFT does not improve at its spectral estimate with an increase in frequency domain resolution (Percival and Walden, 1993). Frequency domain resolution refers to the length of the analyzed record and the sampling interval. Another spectral analysis technique is the Multi Taper Method (MTM). MTM uses multiple tapers which act as windows to analyze a spectral record (Jeyaseelan and Balaji, 2015). This method excels at determining the amplitude of non-stationary frequencies which are not constantly present through time. MTM is best when the analyzed record is considerably longer than the frequencies being examined or there is a small sampling interval because it improves with increased frequency domain resolution. That is to say the analysis is best on a record that captures several complete cycles of a frequency. For example, MTM will capture a 10 year^{-1} frequency better in a 100 year record where the 10 year^{-1} cycle has occurred 10 times, than a 20 year record where the same cycle has only occurred twice. The best way to demonstrate the two spectral analysis techniques is through the construction of a synthetic signal and then spectral analysis of the signal (Figure 5). With synthetic data it is possible to see the amplitudes of the cycles in Figure 5 (d,e,f,g,h,i). With each additional cycle that is added to a combined signal, it becomes harder to interpret what cycles comprise the combined signal. This is the reason spectral analysis is necessary, it deconstructs the signal and shows what cycles are affecting the data and to what extent. Figure 6 shows the spectral analysis of a combined signal based on the waves in Figure 5 (a,b,c). The FFT of Figure 6 is better at capturing the amplitudes of the frequencies in the synthetic signal because the frequencies are stationary. For all results and discussion, we use MTM spectral analysis since this is the better method for characterizing the non-stationary nature of the climate system.

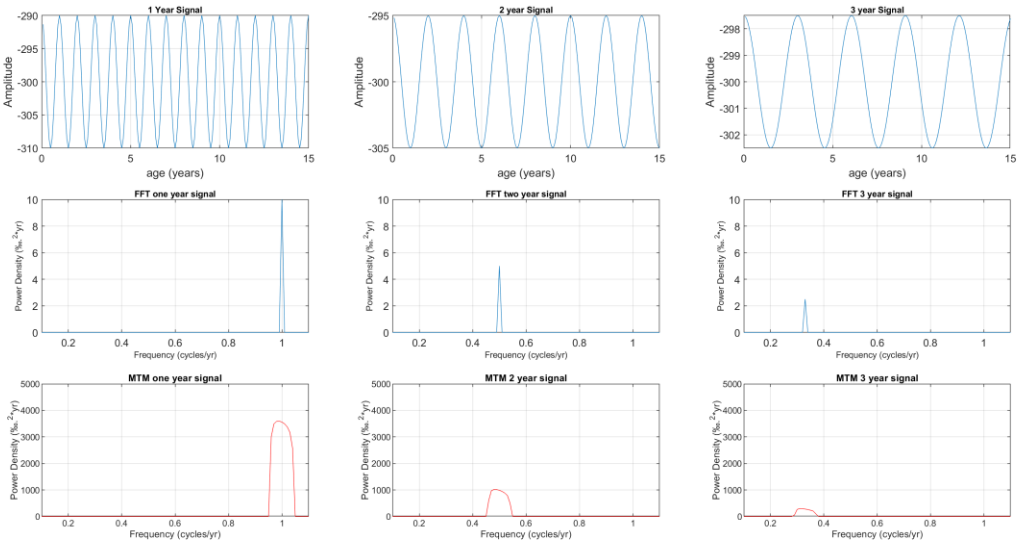

Figure 5: (Top row from left to right) 3 signals and the results of spectral analysis of each individual signal. (a) The first signal has an amplitude of 10 and a frequency of 1. (b) The second signal has an amplitude of 5 and a frequency of 0.5. (c) The third signal has an amplitude of 2.5 and a frequency of 0.33. These 3 signals comprise a 1, 2 and 3 year^{-1} cycles respectively. (Middle row from left to right) The FFT of the signals in the top row. (d) The first FFT is the 1 year^{-1} signal. (e) The second FFT is the 2 year^{-1} signal. (f) The third is the FFT of the 3 year^{-1} signal. FFT returns the exact amplitude of each signal. (Bottom row from left to right) The MTM of the signals in the top row. (g) The first MTM is of the 1 year^{-1} signal. (h) The second MTM is of the 2 year^{-1} signal. (I) The third is the MTM of the 3 year^{-1} signal. MTM returns the relative amplitude of each signal.

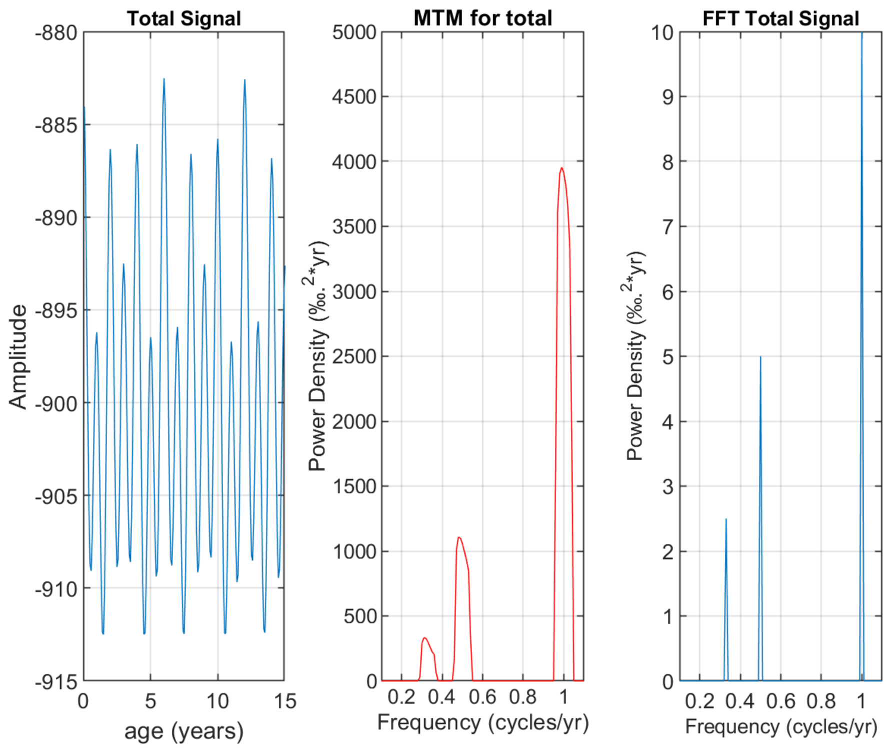

Figure 6: (left) The combined signal of the 1, 2, and 3 year-1 frequencies. (middle) the MTM of the total signal. (right) The FFT of the total signal.

In a real ice core system, the water isotopes represent not only temperature but also regional and local atmospheric circulation as well as diffusion. It is necessary to understand the different types of spectral noise and how they affect spectral estimates. There is red, white, and blue noise. Each color of noise is distinguished by a different relationship with frequency (Wunsch, 2003; Fisher et al 1985). Red noise has less power density as frequency increases. White noise is non-dependent on frequency and does not increase or decrease with frequency. It is considered a random process. Blue noise has more power density as frequency increases. In an ice core, red noise occurs from diffusional processes in the firn, and white noise usually occurs at frequencies not affected by diffusion and resulting from random weather patterns. Ice cores water isotopes do not exhibit blue noise. See Figure 11 for additional information.

Section 3: Results

Spectral analysis is a vital tool for understanding the climate cycles that govern a paleoclimate proxy record. With spectral analysis it is possible to discover the periodicities present in a paleoclimate record which could correspond to forcing mechanisms that govern the changes seen in that record. To illustrate this, we provide a few examples of spectral analysis in previously published climate records: 1) the LR04 benthic stack (Lisiecki and Raymo, 2005) and 2) Nino 3.4 temperature data. Later, the same type of spectral analysis is done on the WDC and SPC water isotope records.

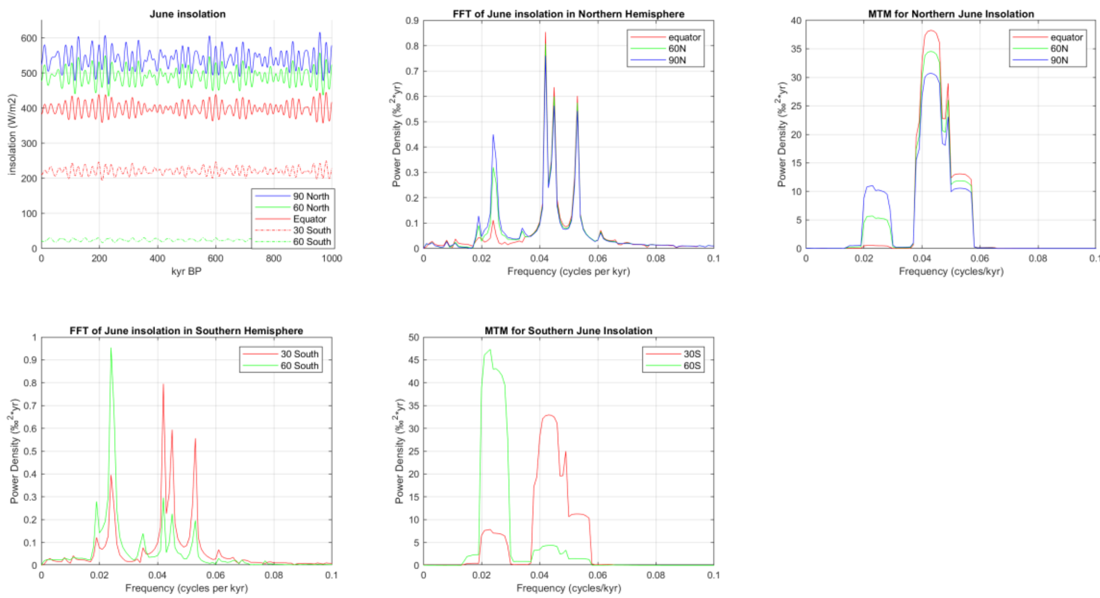

Figure 7: (top left) June insolation derived from the LR04 benthic stack for the last million years. (top middle) FFT of the June insolation is done for the equator, 60 degrees North, and 90 degrees North. (top right) MTM spectral analysis is performed on the same dataset. (bottom left) FFT of southern insolation. (bottom right) MTM spectral analysis of southern insolation. The spectral analysis of the graphs reveals frequencies of 0.024, 0.053, 0.045, and 0.042 kyr^{-1} that correspond to a 41,000, a 23,000, a 22,000, and 19,000 year cycle. These periodicities correspond to the obliquity cycle and the three periodicities of precision. The colors of each frequency reveal how strong each cycle is at different latitudes. The color that is at the top of a peak corresponds to the latitude that was most affected by that frequency.

3.2. Examples of Spectral Analysis in Climate Records

3.2.1. Benthic stack (ocean sediment)

Climate records that include long wavelengths, such as the LR04 Benthic stack, can detect Milankovitch cycles and show how some places on Earth are more affected by obliquity than precession. For example, Figure 7 shows how the poles are more affected by obliquity (41,000 year cycle) whereas the equator is modulated through precession (19,000, 22,000 , 23,000 year cycle) the most. This is shown by the poles having a higher power density at the .024 kyr^{-1} frequency and the equator having a higher power density at the frequencies that correspond to precession.

The benthic stack shows the $\delta^{18}O$ variability of benthic foraminifera during the last 800 kya. It is a stack record because it is an amalgamation of many smaller foram records that were put together to create one record that spans 800ka. Foraminifera are another paleoclimate proxy, they are single celled organisms that make their shell out of calcite. The calcite is precipitated from the ocean water and becomes part of the shell. Just like with ice cores, there is fractionation that happens during this process that is temperature dependent. By looking at $\delta^{18}O$ or another foram proxy, mg/ca, temperature can be deduced. Benthic foraminifera are bottom water dwellers and thus reflect changes in temperature at the ocean's bottom. Spectral analysis of this record reveals what cycles control the bottom water temperatures. Figure 8 shows the spectral analysis of the benthic stack. The ocean responds to some of the same forcing that are seen in ice cores such as the Milankovitch cycles. The spectral analysis reveals the periodicity of Milankovitch cycles with the largest being the eccentricity (100,000 year cycle, .01 kyr^{-1}) and then obliquity (41,000 year cycle, .024 kyr^{-1}) and then the precession cycles (19,000, 22,000, 23,000 year cycle, 0.053, 0.045, and 0.042 kyr^{-1}).

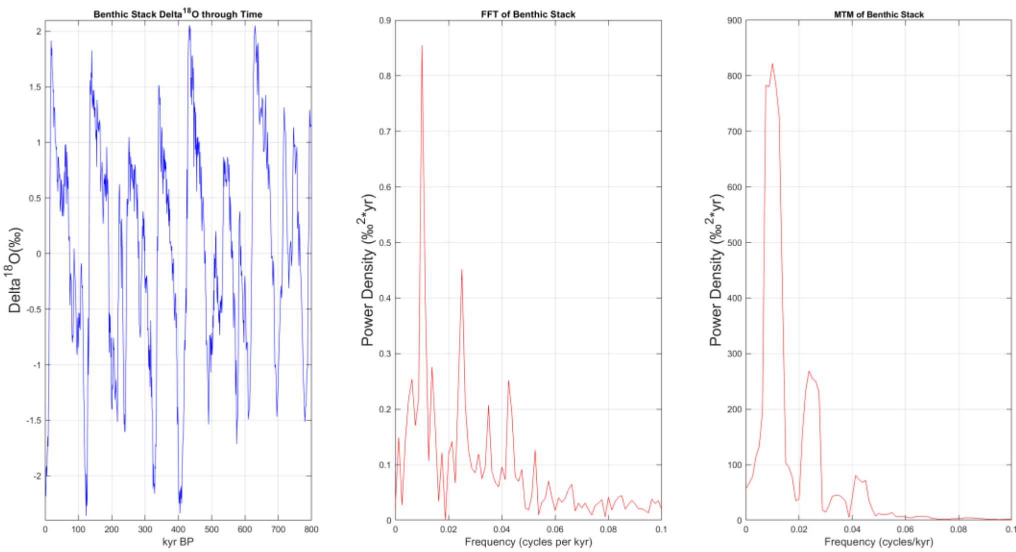

Figure 8: (left) LR04 Benthic stack $\delta^{18}O$ through the last 800 ka. (Middle) FFT of benthic stack. (Right) MTM of benthic stack.

3.2.2. ENSO:

Another example where spectral analysis is useful is for understanding the El Nino Southern Oscillation (ENSO). ENSO represents a reorganization of atmospheric and oceanic currents in the tropical Pacific with globally propagating teleconnections. The ENSO teleconnections result in some areas of the Earth becoming hotter and drier than usual and others wetter. A historic dataset to use for finding the 2-7 year^{-1} signal of ENSO is the Nino 3.4 monthly mean sea surface temperatures (SST) and the Nino 3.4 monthly mean sea surface temperature anomalies (Trenberth, 1997). This dataset covers an area from 120° to 170° West and 5° North and South of the equator. Because ENSO is quasi-periodical (not a singular set periodicity) there are several peaks representing the cycle which are shown through spectral analysis. FFT is a better fit for this dataset because there is a low frequency domain resolution due to how few cycles of ENSO are completed in the 32 year dataset (Figure 9). The superior ability of MTM to capture the non-stationarity of ENSO is seen through the Southern Oscillation Index (SOI), which is a measurement of the air pressure difference between Tahiti and Darwin, Australia (Figure 10). El Nino changes oceanic and atmospheric circulation in these areas which result in a negative pressure difference between the two whereas La Nina years result in a positive difference. The length of this dataset is longer than the Nino 3.4 dataset which correlates to a higher frequency domain resolution. FFT weighs all oscillations equally whereas MTM weighs dominant oscillations more heavily than short term oscillations. Because of this, MTM captures the non-stationary quasi-periodic ENSO frequencies while FFT displays these frequencies and non-target frequencies.

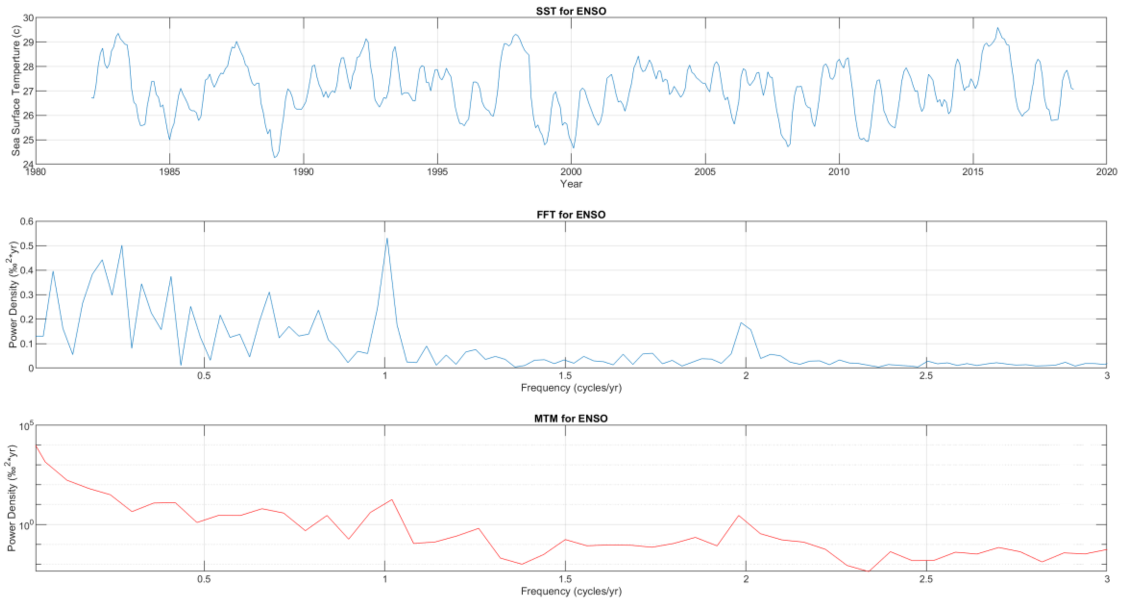

Figure 9: (top) Sea surface temperature for Nino 3.4. (middle) FFT of Nino 3.4. (top) MTM of Nino 3.4 with a y log scale.

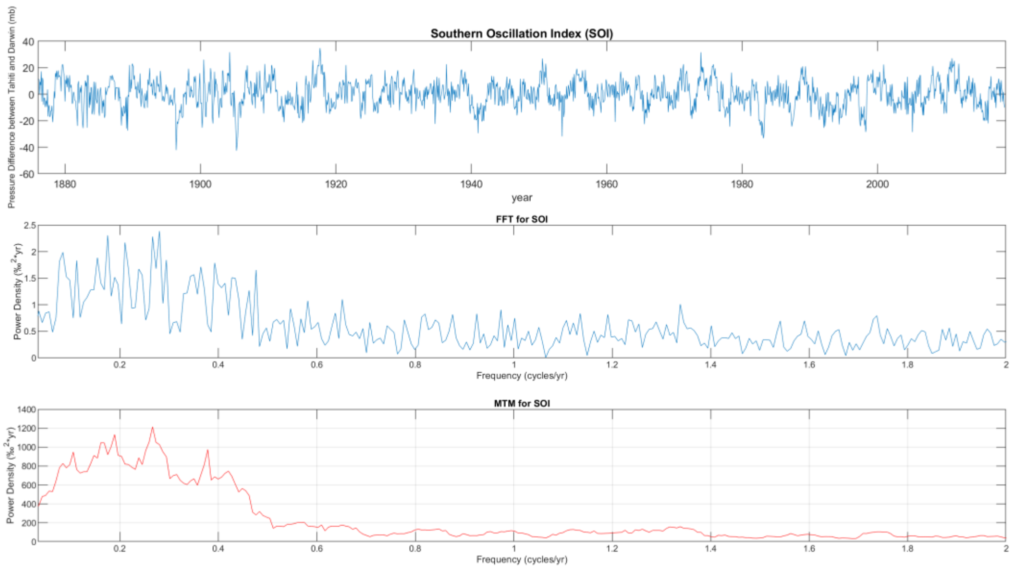

Figure 10: (top) Southern Oscillation Index pressure differences between Tahiti and Darwin. (middle) FFT spectrum of the SOI. (bottom) MTM spectrum of the SOI.

3.3. Antarctic Ice Core Records

3.3.1. Spectral analysis

This study analyzed the South Pole ice core (SPC) and WAIS Divide ice core (WDC). WDC goes back 67 thousand years and SPC extends to 54.2 thousand years ago. Figure 11 and Figure 12 show the δD and δ^{18}O of both records and the mean values of each. Each record has a sampling resolution of 20 samples per year, which allows for high frequency (multi-year and decadal) signals to be analyzed. Figures 13 and 14 show the spectrum of WDC and SPC records as well as what type of noise each is impacted by. The 1 year^{-1} frequency is seen as a large spike. White noise is seen as a flat line and associated with random weather events. White noise occurs at frequencies between the 10 year^{-1} to 250 year^{-1} frequencies. Instrumental noise is seen in the drop off in sub-annual frequencies. Frequencies higher than 10 year^{-1} have climate variability that exhibits red noise as a result of diffusion. Frequencies lower than 250 year^{-1} also exhibit red noise.

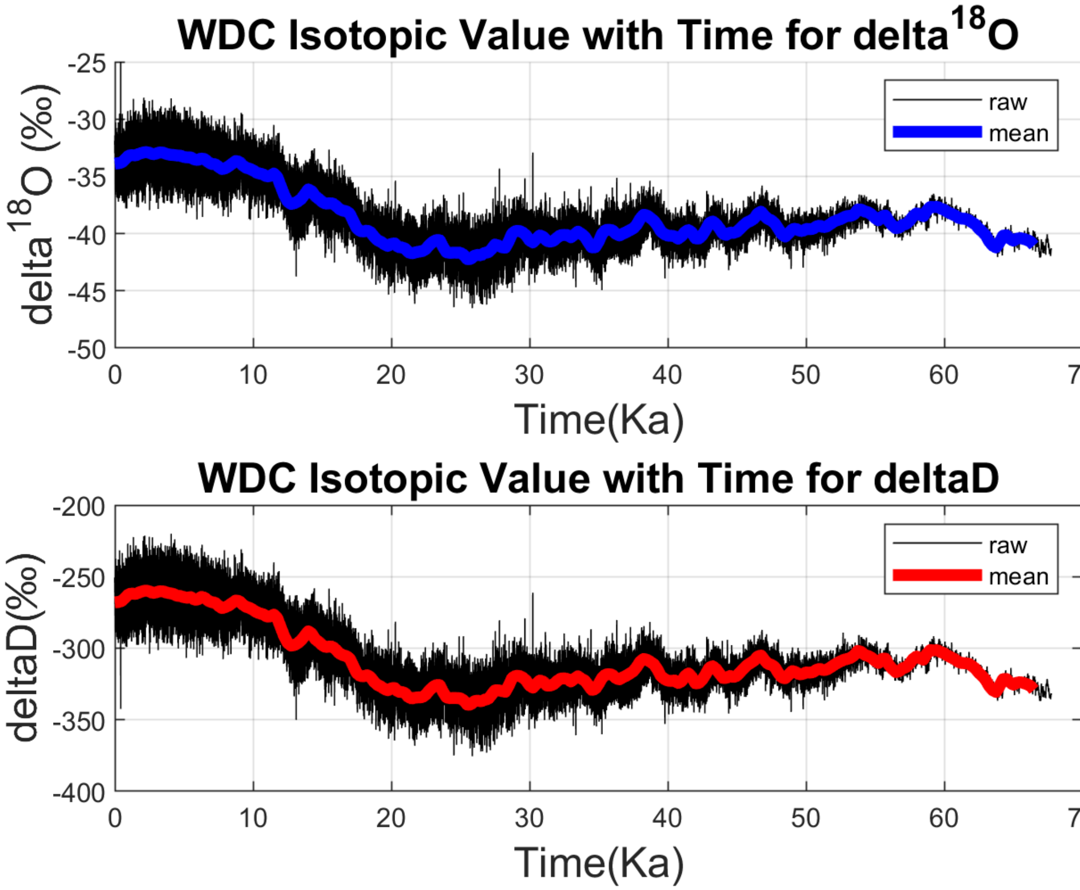

Figure 11: δD and δ^{18}O of WDC throughout the record. The blue and red lines are the mean values taken from a 500 year sliding window through time.

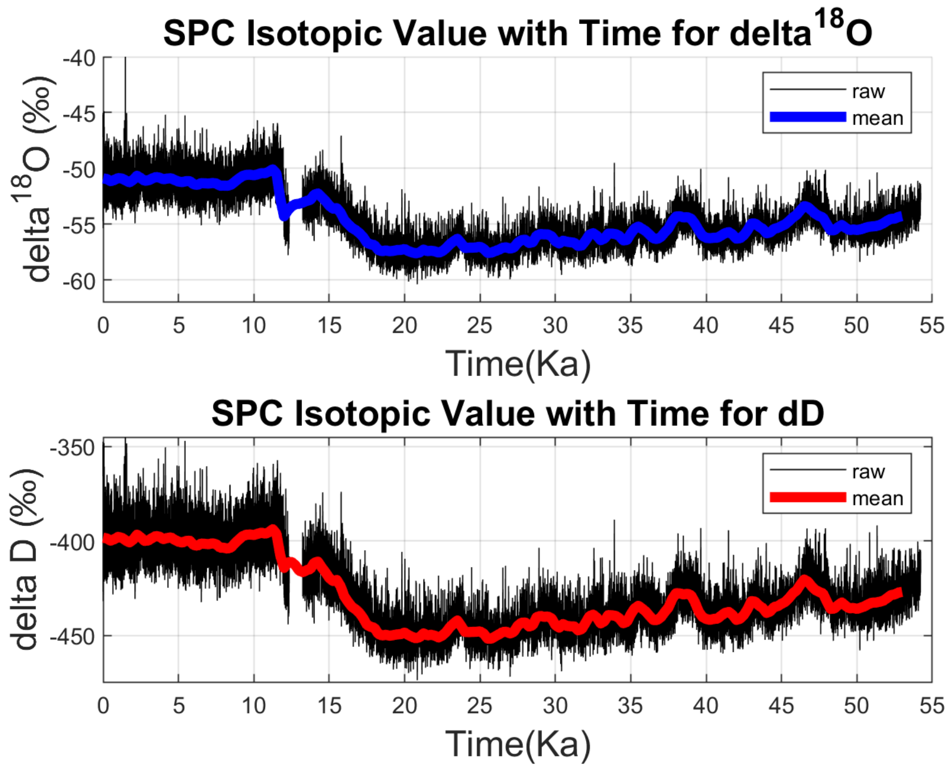

Figure 12: δD and δ^{18}O of SPC throughout the record. The blue and red lines are the mean values taken from a 500 year sliding window through time. There is missing data from 12.34 ka to 13.24 ka.

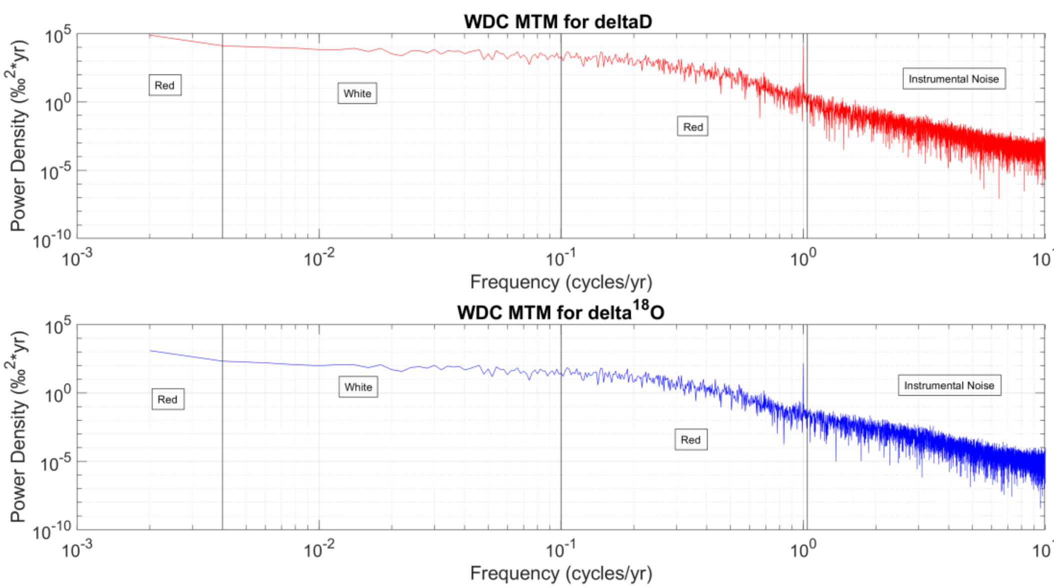

Figure 13: spectral spectrum for δD and δ^{18}O of the WDC record. Results obtained through MTM spectral analysis.

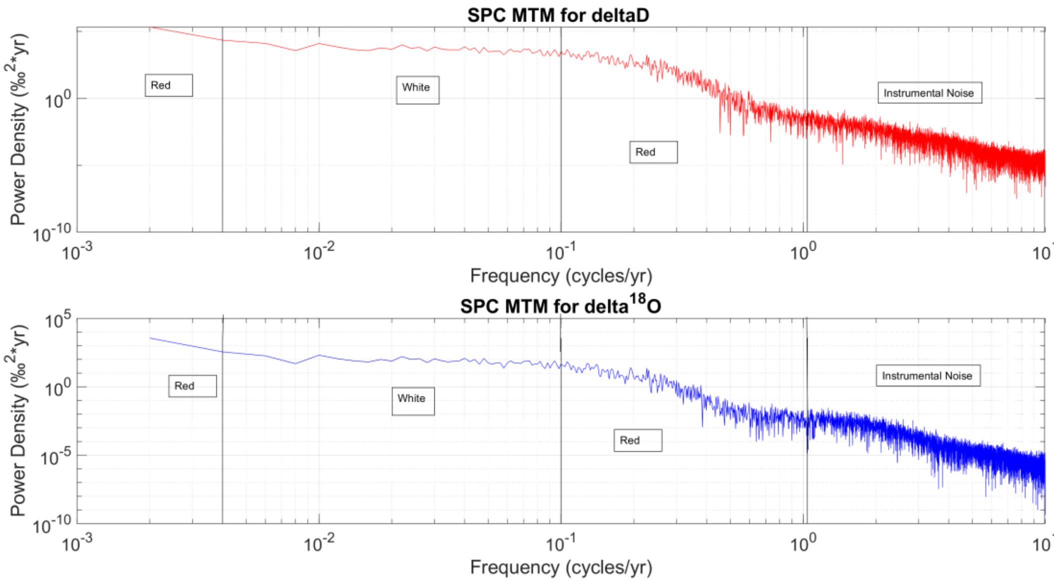

Figure 14: spectral spectrum for δD and δ^{18}O of the SPC record. Results obtained through MTM spectral analysis.

3.3.3. WDC first order diffusion analysis:

The results from this study are not corrected for diffusion. This limits interpretation of the core but can be accounted for in the analysis. The power densities of each frequency reflect the climate and diffusion. Diffusion influences higher frequencies the most and has a larger impact on older ice as well as times when accumulation on the ice sheet was lower. Diffusion will impact the 1 year^{-1} frequency the most, and due to low accumulation rates, completely eliminate the annual signal during glacial times. The annual signal is lost at WAIS Divide around 16ka and is not recorded at the South Pole. Four and greater year^{-1} frequencies are preserved but still impacted by diffusion. Although the 2 year^{-1} signal is nearly lost between 15 and 17 ka, it and the 3 year^{-1} become fully lost at 40 ka (Figure 15). Figures 16, 17, and 18 show the diminishing role of diffusion with increasingly lower frequencies. Using these figures, it

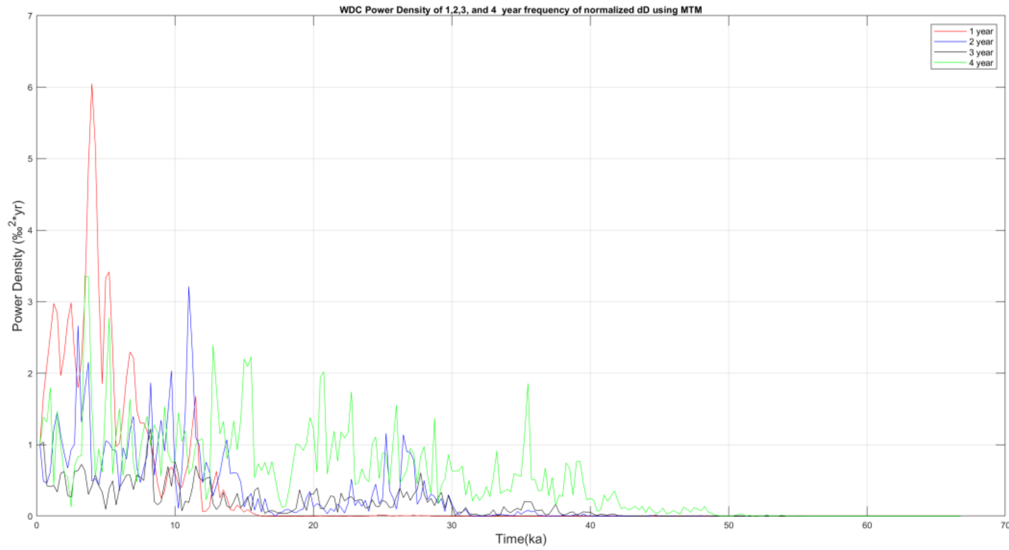

Figure 15: Normalized using the mean amplitude of each frequency of the first 500 year window, δD signal of the 1, 2, 3, and 4 year^{-1} using MTM analysis. The 1 year^{-1} is red and disappears at 16ka. The 2, 3, and 4 year^{-1} signals are blue, black, and green respectively.

becomes clear which signals are retained and which are lost. Figures display frequency signals of δD and not δ^{18}O because it diffused less in the firn column and therefore better suited for analysis of changes in power density. All δD signals have been normalized to the mean value of the amplitude of their respective frequencies from the first 500 year window of MTM spectral analysis. The dln has also been normalized but the 5th value was used instead.

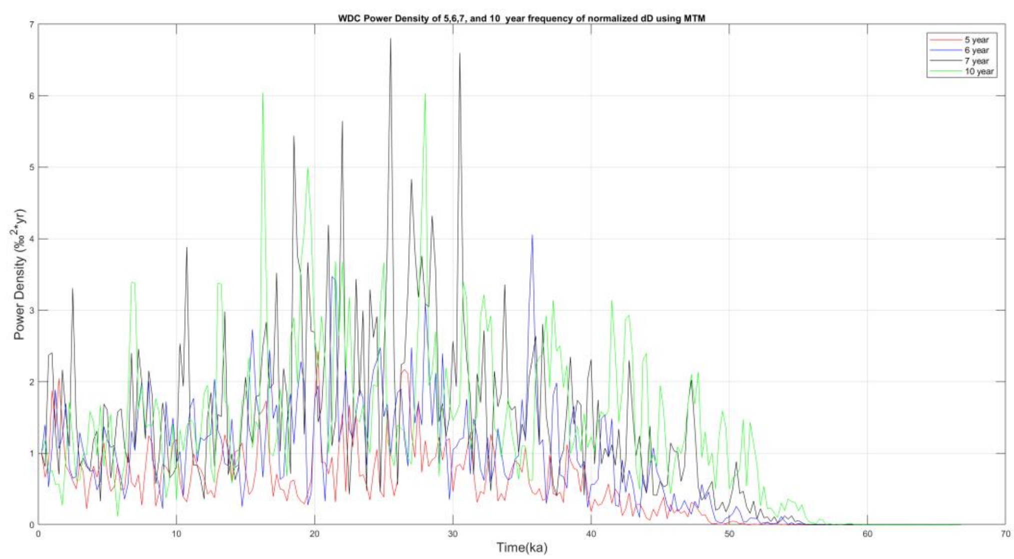

Figure 16: Results of normalized MTM spectral analysis of the 5, 6,7, and 10 year^{-1} signal seen as red, blue, black, and green respectively. The 5 and 6 year^{-1} signals are impacted by diffusion significantly more than the 7 and 10 year^{-1} signal.

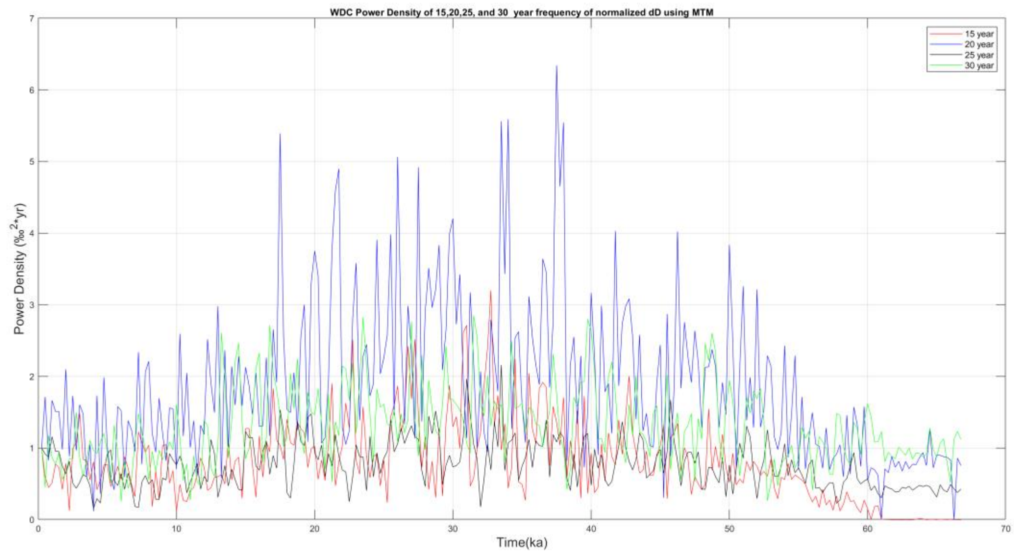

Figure 17: Results of normalized MTM spectral analysis of the 15, 20, 25, and 30 year^{-1} signal seen as red, blue, black, and green respectively. The 20 year^{-1} has the largest power density values.

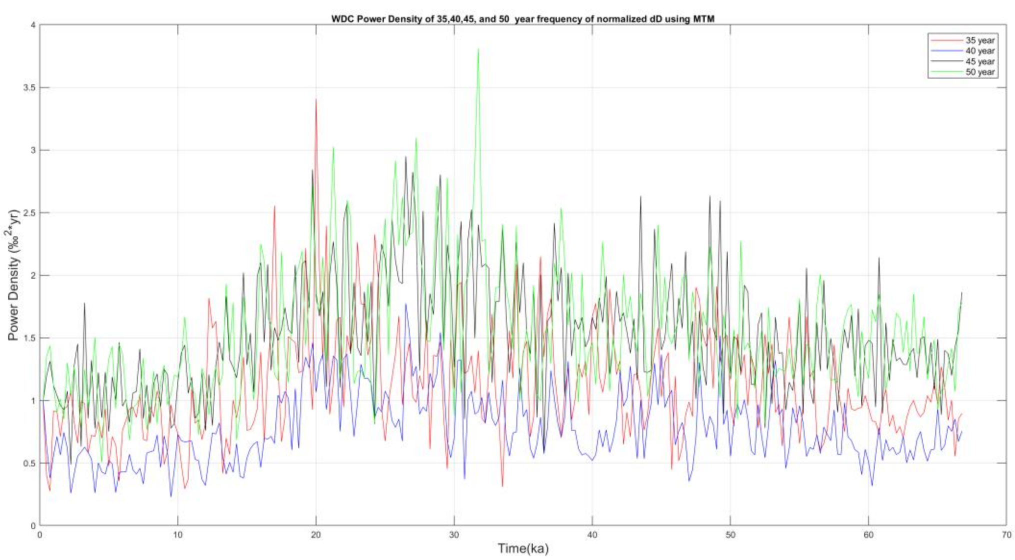

Figure 18: Results of normalized MTM spectral analysis of the 35, 40, 45, and 50 year^{-1} signal seen as red, blue, black, and green respectivly.

3.3.4. SPC first order diffusion analysis:

Figures 19 through 22 show the results of numerous single frequency bands plotted together on a power density with time plot. The results are similar to figures 15 to 18 of the WDC graphs. The differences between these sites are notable in the comparison of figures 15 and 19. Unlike WDC, SPC has lower accumulation and more diffusion leading to high frequencies being eliminated. We see this in Figure 19 with the loss of the 1,2, and 3 year^{-1} signals. Figure 15 shows the same frequencies through time at the WDC site. At SPC, the 1,2, and 3 year-1 signals are eliminated before 16ka. At WDC, only the 1 year^{-1} signal is eliminated at 16 ka, while the 2 and 3 year^{-1} are eliminated at 40 ka. The greater effects of diffusion at the SPC site is seen through figures 19 to 22 all having smaller power densities throughout time than their WDC counterparts. The exception to this is the 7 and 10 year^{-1} signals from SPC which are higher than WDC 7 and 10 year^{-1} signals. respectively. The 7 and 10 year^{-1} signals are impacted by diffusion significantly less than the 5 and 6 year^{-1}.

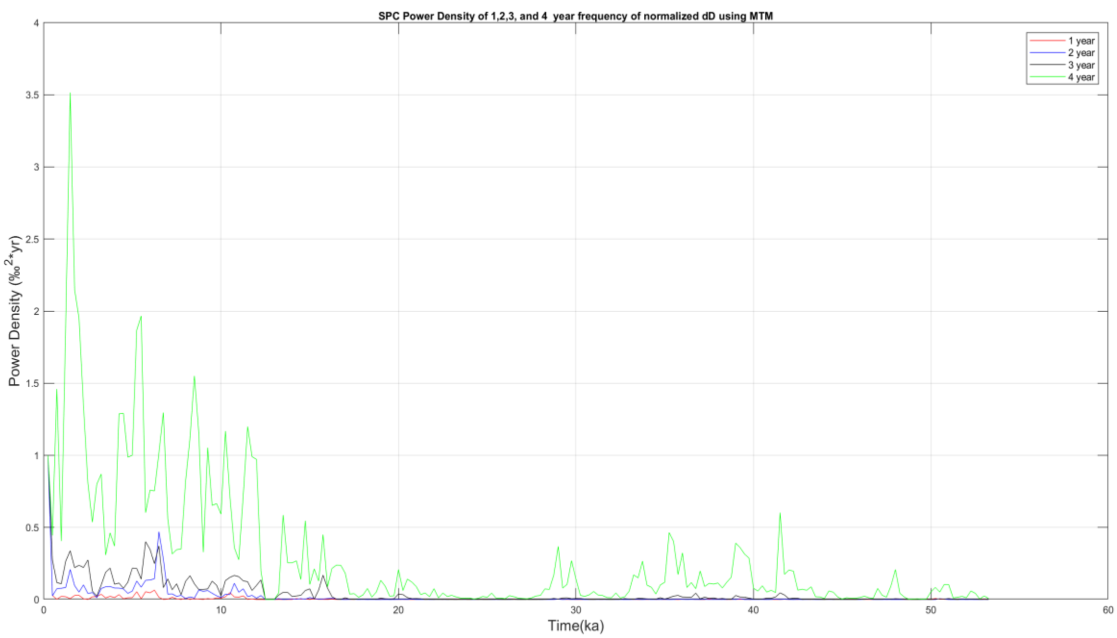

Figure 19: Normalized δD signal of the 1, 2, 3, and 4 year^{-1} frequencies using MTM analysis at SPC core. The 1,2, and 3 year^{-1} signals all disappear before 16 ka and are heavily influenced by diffusion. The 4 year^{-1} signal is possibly seen throughout the record but this interpretation is questionable due to there being a 10,000 year period of power density values of zero.

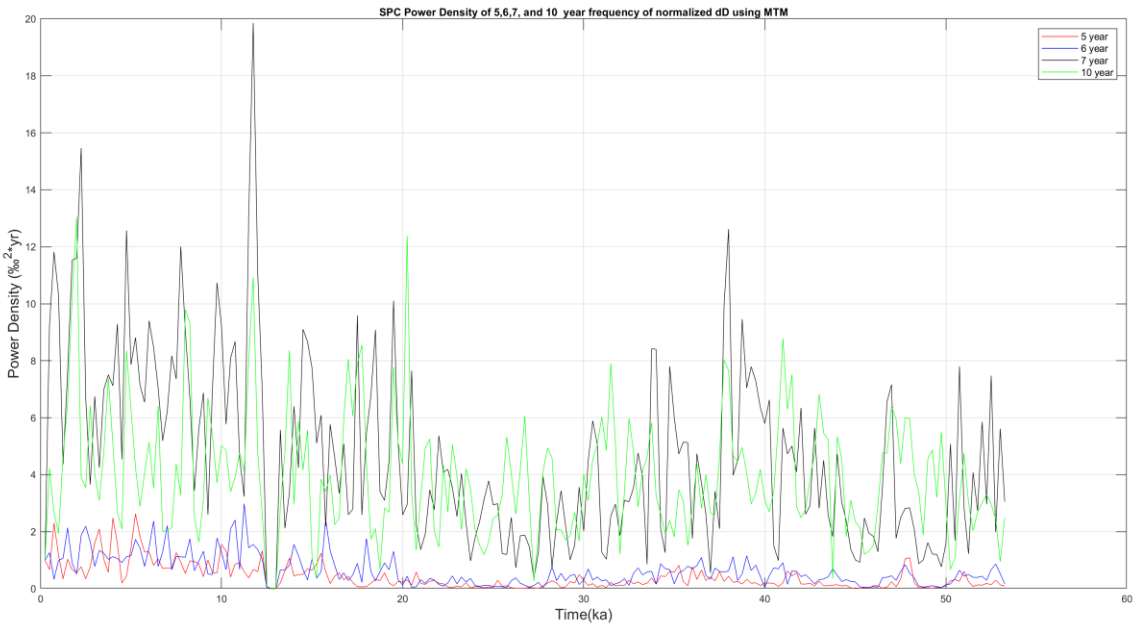

Figure 20: Normalized δD signal of the 5, 6, 7, and 10 year^{-1} frequencies from the SPC using MTM spectral analysis. The 5,6,7, and 10 year^{-1} frequencies are shown as red, blue, black, and green [1].

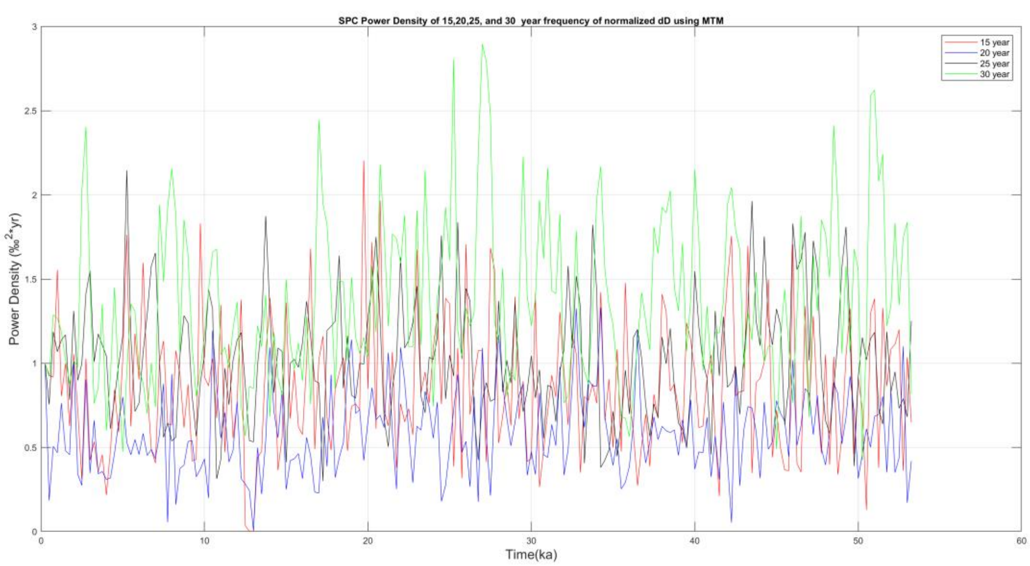

Figure 21: Normalized δD signal of the 15, 20, 25, and 30 year^{-1} frequencies from the SPC using MTM spectral analysis. The 15, 20, 25, and 30 year^{-1} frequencies are shown as red, blue, black, and green respectively.

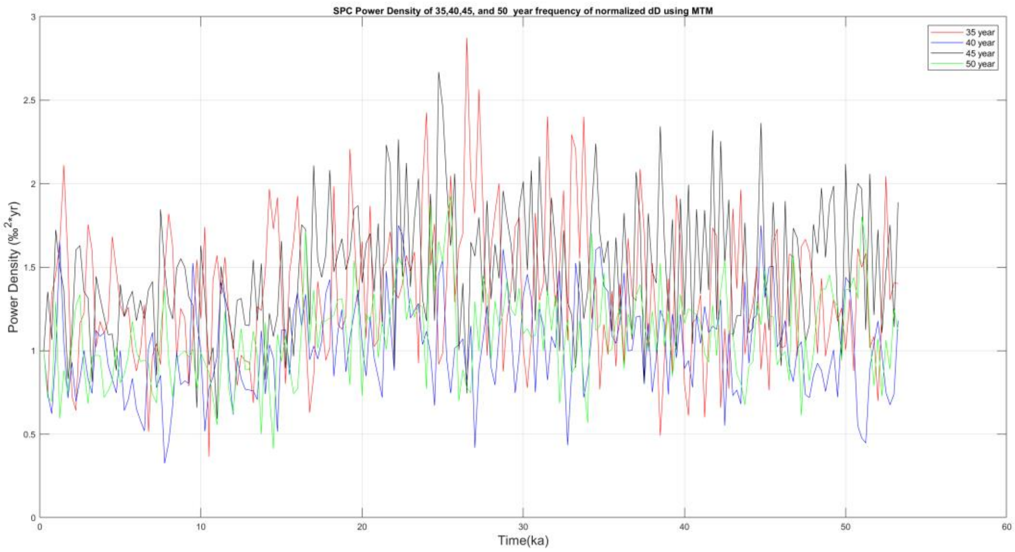

Figure 22: Normalized δD signal of the 35, 40, 45, and 50 year^{-1} frequencies from the SPC using MTM spectral analysis. The 35, 40, 45, and 50 year^{-1} frequencies are shown as red, blue, black, and green respectively.

3.3.5. Diffused signal summary:

The WDC frequencies are less affected by diffusion than SPC, due in-part to higher accumulation rates at WDC. WDC signals with wavelengths less than about 7 years are substantially affected by diffusion and must be interpreted with this in mind. Diffusion should be taken into account for frequencies up to about 15 year^{-1} . Frequencies lower than 15 year^{-1} can be interpreted primarily in terms of a climate signal. After about 40 ka, thermal diffusion impacts all frequencies at WDC and SPC which severely limits interpretation. A full diffusion modeling effort would be necessary to understand exactly how all frequencies are affected, and the suggestions above are based in part on Jones et al. (2017, 2018). The larger diffusional effect at SPC is seen by lower frequency bands being affected by diffusion at SPC than WDC. For example, the WDC 4-15 year^{-1} band is not affected by diffusion (Figure 25) whereas the SPC 4-15 year^{-1} band is impacted by diffusion (Figure 29). The diffusional impact is seen in the SPC 4-15 year^{-1} frequency band through higher power density during the Holocene than during 20 to 30 ka, a period that usually contains the highest power density values. At SPC, up to the 4 year^{-1} frequency is lost completely. Although not eliminated, up to the 7 year^{-1} is heavily impacted by diffusion and analysis of frequencies up to 15 year^{-1} should be interpreted with diffusion in mind. These conclusions are based off of a first order technique to interpret general diffusional influences on frequencies but are all assumptions and cannot be confirmed without diffusion corrections made with diffusional modeling.

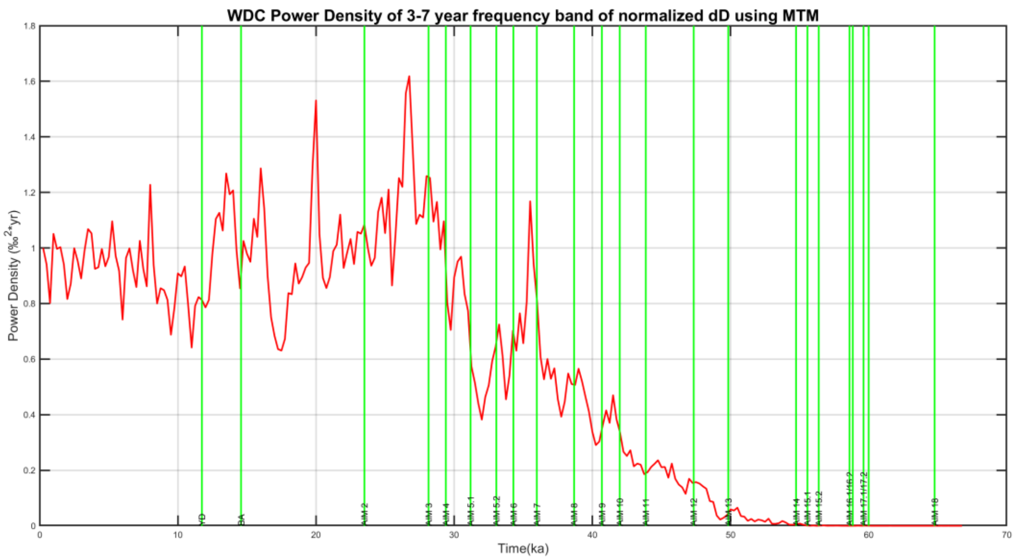

Figure 23: Results of normalized δD MTM spectral analysis of the 3 to 7 year^{-1} frequency band from WDC. Diffusion plays a significant role after 31ka.

Section 4: Discussion

4.1.1. Site descriptions

This study analyzes the South Pole Ice core (SPC) and WAIS Divide ice core (WDC). Figure 24 shows the geographic locations of both with SP marking SPC and WD marking WDC. WDC has a coastal signal that is tied to changes in the Pacific Ocean. SPC is continental and could be influenced by multiple ocean basins. In addition, it has less accumulation than WDC and thus is more impacted by diffusion.

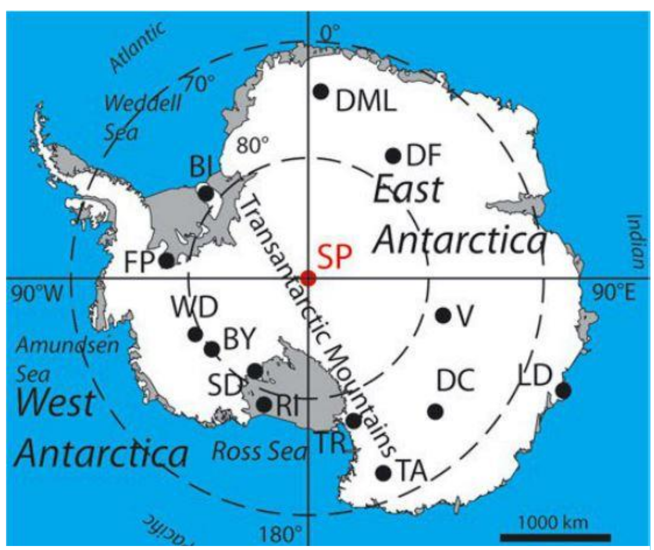

Figure 24: Ice cores of Antarctica (phys.org 2015)

4.1.2 WDC

The 4 to 15 year^{-1} frequency band for WDC is composed of three steps and three regime shifts. Steps characterize periods of time where the power density hovers around a single average value and regime shifts are characterized as periods of time where the average power density is increasing or decreasing. From the present to 8 ka the signal is relatively constant and contains little variability. There is a pronounced trough at 9.5 ka and a regime shift from there until 16 ka. The next step is from 16 to 31 ka with slowly increasing power density values further back in time. At 31 to 37 ka there is another regime shift to smaller power density values. The third step is relatively constant values from 32 to 36 ka. An important feature of the signal is a prominent spectral peak at 20 ka. Another feature of the WDC 4 to 15 year^{-1} signal is a substantial decline at time periods greater than 40 ka. A known physical process that affects the WDC is thermal diffusion arising from basal geothermal heating (Fisher et al. 2015). While this effect is small, over time it can substantially diffuse the high frequencies of the isotope record. We can not reliably interpret ages greater than 40 ka due to this added diffusional effect which would require a number of modeling approaches to reconcile. The analysis can be extended past 40 ka for lower frequencies that are less susceptible to diffusion but not for the WDC 4 to 15 year^{-1} frequency band.

While analysis of individual frequencies is useful to understand the combination of diffusion and climate signals, the use of frequency bands gives a better indication of how the climate is acting across many frequencies. In Jones et al. (2018), the authors note that the WDC 3 to 7 year^{-1} band (Figure 23) is substantially influenced by diffusion while the WDC 4 to 15 year^{-1} band (Figure 25) is more representative of the climate signal. Jones et al. (2018) determined that the 4 to 15 year^{-1} band was influenced by the topography of the Laurentide ice sheet and the ice sheet's effect on atmospheric circulation and teleconnection mechanisms between western Antarctica and the tropical Pacific. For the first time, we extend the analysis beyond 30 ka. One of the interesting implications is that we would expect with a smaller Laurentide ice sheet, the strength of the 4 to 15 year^{-1} band should decrease. Reconstructions of the Laurentide ice sheet (Dalton et al. 2019) show that the ice sheet was growing at 31 ka, thus we would expect the power density to be lower at years older than 31 ka when the Laurentide was smaller. We see this in Figure 25 with the strongest signal for 4 to 15 year^{-1} occurring from about 16 to 31 ka but is lower from 31 to 40 ka for example. This is consistent with the effect of the Laurentide ice sheet on Western Antarctica and corroborates the Jones et al. (2018) study. Better constraints on the size of the Laurentide ice sheet would help determine the relationship between the ice sheet and the 4 to 15 year^{-1} band at ages older than 31ka. Future diffusion corrected studies should investigate the 31 to 40 ka section of the 4 to 15 year^{-1} spectral bands to see if they also observe this decrease after 31 ka. If the decrease is observed, it signifies the signal is low due to climate and not diffusion.

Mapping of AIM events with the 4 to 15 year^{-1} signal was preformed to attempt to determine the correlation between the two. AIM events signify warmer periods in Antarctica and thus would lead to more accumulation. The 4 to 15 year^{-1} band should have higher spectral peaks at this time if only diffusion (and not climate) is considered, since larger annual layers would preserve larger amplitude signals. However, this is not the case as seen in Figure 22.

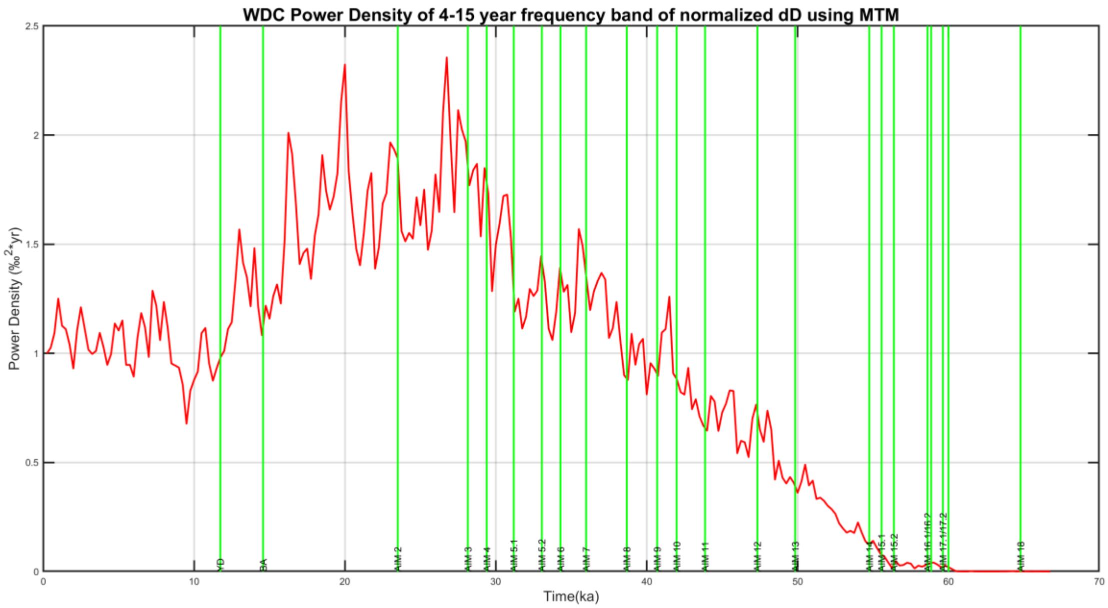

Figure 25: Results of normalized δD MTM spectral analysis of the 4 to 15 year^{-1} frequency band. There is a large drop in spectral power at ages younger than 16.5 ka and another drop at ages older than 30.75 ka. AIM events, the Younger Dryas, and the Bolling-Allerod are plotted as vertical lines on the graph.

Jones et al (2018) focused on the 4 to 15 year^{-1} cycles since these are associated with ENSO which is a known teleconnection between the Tropical Pacific and Western Antarctica. Other frequency bands are important to interpret but may not provide the same information about the climate system. The WDC 15 to 30 year^{-1} band (Figure 26) shows similar results to the 4 to 15 year^{-1} in that it is low from 0 to 10 ka and increases from 16 to 31 ka, however unlike the 4 to 15 year^{-1} signal the 15 to 30 year^{-1} band does not substantially decrease from 31 to 40 ka which suggests a different forcing mechanism that is not well understood. The diffusion effect is smaller for these frequencies as well. It is possible that the decrease seen in the 4 to 15 year^{-1} band drops in power density at 31 ka as a result of diffusion and can be corrected for in future studies. This interpretation is unlikely due to diffusion not impacting the lower frequencies much at this time.

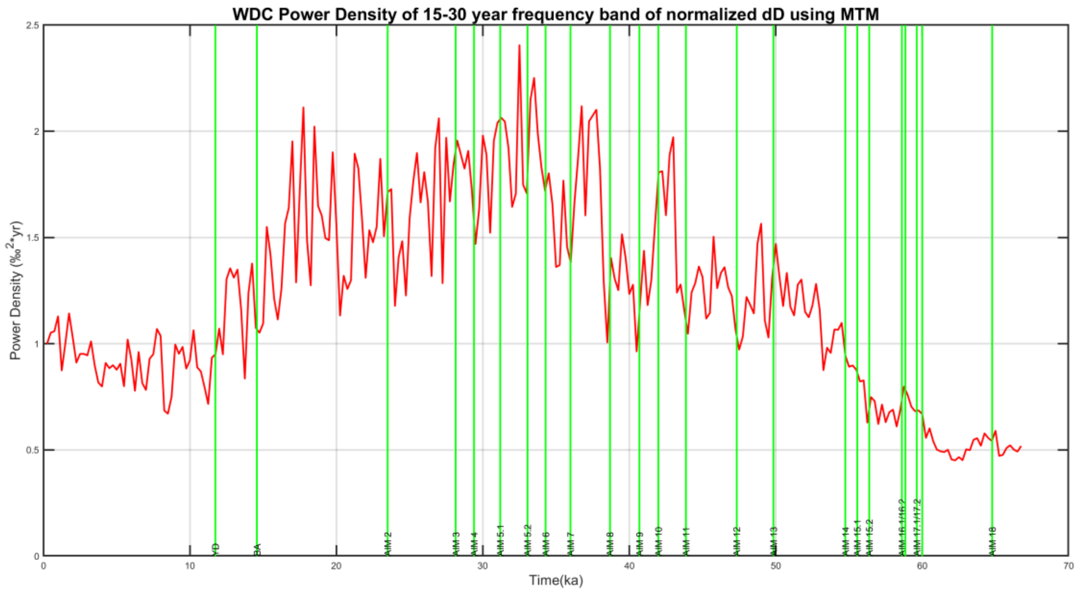

Figure 26: Results of normalized δD MTM spectral analysis of the 15 to 30 year^{-1} frequency band. There is a large drop in spectral power at ages younger than 16.5 ka and another drop at ages older than 37.75 ka. AIM events, the Younger Dryas, and the Bolling-Allerod are plotted as vertical lines on the graph.

The data from the WDC 15 to 30 year^{-1} frequency band contains a step like trend with some periods of regime shifts. The first step is from the present to the Younger Dryas at 11.75 ka. This step has little variability and low power densities. Afterwards there is a regime shift from 12 to 16 ka where the overall signal rises in both power density and variability. The second step is from 16 to 24 ka and experiences more variability in power density than the first step. There is a slight increase in power density values in the third step from 24 to 34 ka. From 34 to 38 ka there is another regime shift to a step with lower power densities. The fourth step is from 38 to 53 ka. Diffusion plays a role in the lowering of the fourth step but the observed step like decline is likely a preserved artifact.

There are notable exceptions to the step organization described above. There are three substantial spikes at 32.5, 36.75, and 43 ka in the 15 to 30 year^{-1} frequency band at WDC. These peaks are anomalyous and do not align with AIM events. Future research should investigate other global climate proxies to observe if they correlate. The peaks as well as the fall in power density at 30 ka could relate to ice sheet topography. If the peaks are connected to ice topography it would suggest that an ice sheet can grow significantly in 1500 years.

Although some spectral spikes align with AIM events, the largest peaks do not. Half of the AIM events align with spectral troughs and other events do not line up with troughs or peaks. In addition, there are many fluctuations in power density that are not covered by AIM events. These observations signify that there is no correlation between AIM events and the 15 to 30 year^{-1} frequency band. These results are contrary to what might be expected. AIM events represent times of rapid warming in Greenland and a gradual warming in Antarctica. It therefore may be expected that a high frequency dominated system would occur during AIM events.

There are numerous conclusions that could be reached about the relationship between AIM events and the 15 to 30 year^{-1} frequency band. An improved age scale and higher frequency resolution could improve interpretations. A possible interpretation of this relationship is that despite warming, AIM events may mark a more stable climate in Antarctica than cold times and that the 15 to 30 year^{-1} frequency band corresponds to a forcing mechanism different than AIM events. The AIM events may be governed by low frequency cycles on a millenial scale. High frequencies, such as the 15 to 30 year^{-1} band, do not map to the same multi-thousand year wavelength that the AIM events are controlled by. Potentially the 15 to 30 year^{-1} frequency band could be mapping to variations in the Tropics. This knowledge could improve global circulation models. Investigation about this forcing mechanism is outside the scope of this study and should be looked into in future studies.

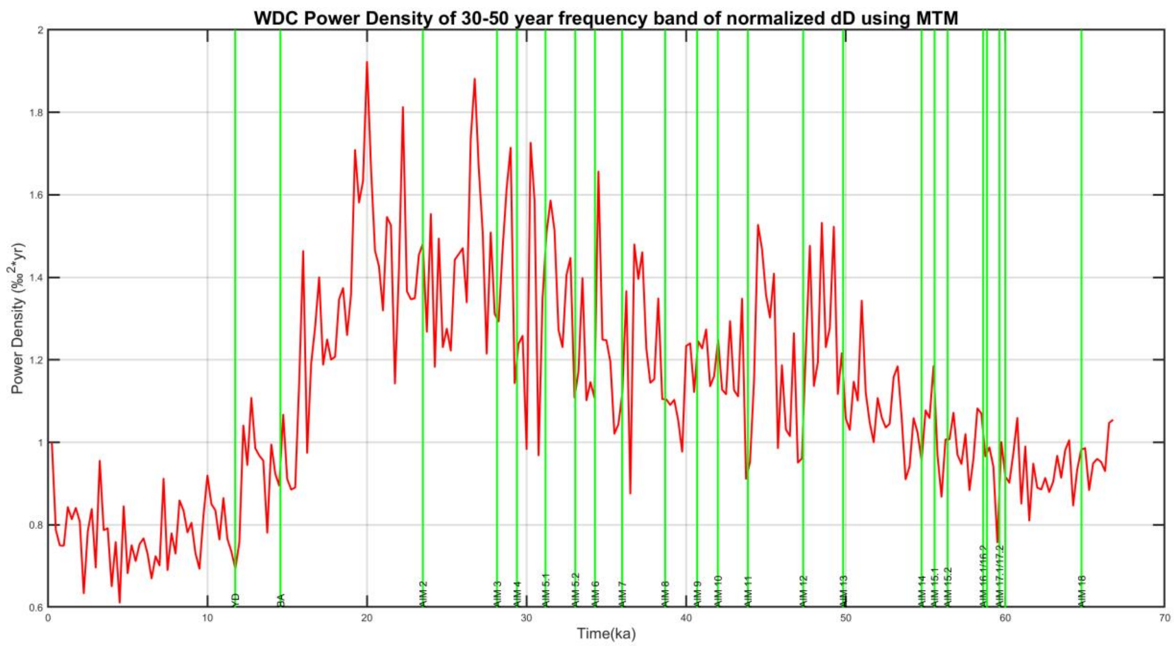

Figure 27: Results of normalized δD MTM spectral analysis of the 30 to 50 year^{-1} frequency band. There is a large drop in spectral power at ages younger than 16.5 ka. AIM events, the Younger Dryas, and the Bolling-Allerod are plotted as vertical lines on the graph.

The 30 to 50 year^{-1} spectral band has a similar pattern in spectral power through time consisting of 3 steps and 2 regime shifts. The first step is from the present to Younger Dryas at around 12 ka. This step is usually lower than the steps in glacial periods but was significantly lower in the 30 to 50 year^{-1} frequencies than in the other investigated frequencies. From the Younger Dryas to 19 ka there is a regime shift to higher power densities. Step 2 has high power density and variability and is from 19 to 31.5 ka. After step 2 there is a regime shift towards lower power density with continued variability. The regime shift lasts from 31.5 to 35 ka. Step 3 is from 35 to 50 ka. After this point there is significant thermal diffusion. There are three substantial spikes in power density through the time series at 20, 26.75, and

34.5 ka. As with the 4-15 $year^{-1}$ and 15-30 $year^{-1}$ WDC band, the 30 to 50 $year^{-1}$ band does not align with AIM events. This correspondence supports the idea of longer term frequencies controlling AIM events and not higher frequencies.

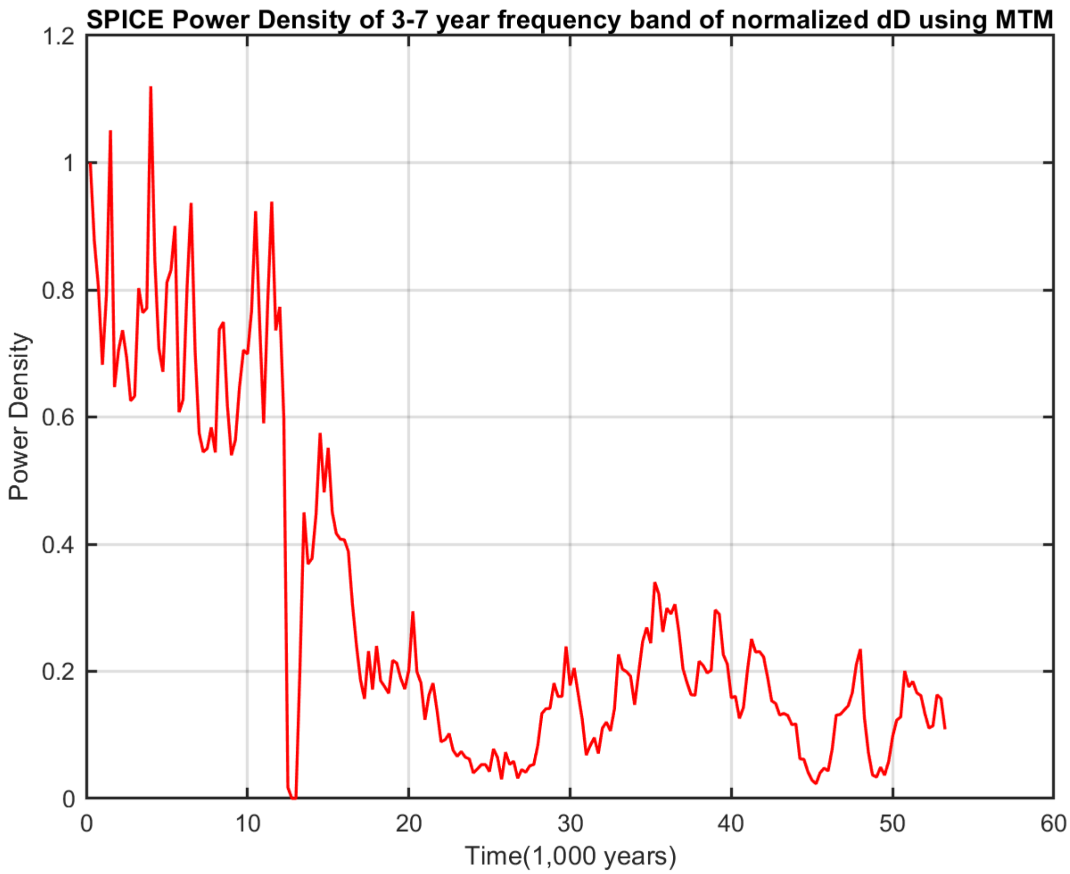

Figure 28: Results of normalized δD MTM spectral analysis of the 3 to 7 $year^{-1}$ frequency band from SPC. The sharp decline in power density around 13 ka is a result of missing data and not representative of a real climate signal.

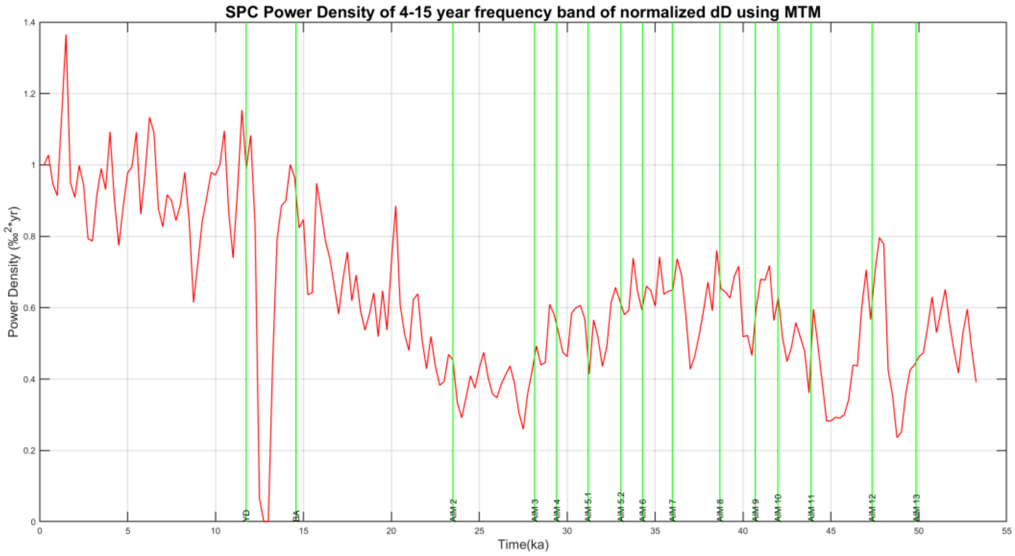

Figure 29: Results of normalized δD MTM spectral analysis of the 4 to 15 year^{-1} frequency band from SPC. The sharp decline in power density around 13 ka is a result of missing data and not representative of actual data.

4.1.3. SPC interpretations:

The results of the 3 to 7 year^{-1} band and 4 to 15 year^{-1} band from SPC show a pattern that could be easily misinterpreted (Figure 28 and 29). The 4 to 15 year^{-1} band shows that Holocene strength of signal is high with a decline into the glacial period. Based on Figure 19 we know that diffusion has a large effect on multi year signals thus this plot represents a mainly diffusional signal but cannot be interpreted much for climate. Instead lower frequencies are required to get an indication of how the climate behaved in the glacial period. Diffusion corrected studies may be able to use the 4 to 15 year^{-1} band to gather information about the climate. Despite the diffusion, a notable spike at 20 ka is still significant.

Figure 30 of the 15 to 30 year^{-1} band is a more realistic representation of climate. Similar to WDC, the signal is lower in the Holocene, higher in mid glacial, and lower later on. The steps in SPC have a smaller difference in power density and overall power density is smaller. Step 1 has the lowest power density and ranges from the present to 14.25 ka. There is then a step change from 14.25 to 19.25 ka. Step 2 contains the highest power density values and occurs from 19.25 to 25.75 ka. There is no long-lasting regime shift between step 2 and 3, instead there is an abrupt decline and transition to step 3 at 25.75 ka. Step 3 last from 25.75 to 34.5 ka. Afterwards there is a regime shift from 35.5 to 46.25 ka with an increasing power density trend. Step 4 has the second highest power density values and goes from 46.25 to 53.25 ka. Prominent spectral peaks occur at 20, 25, 32.75, 33.75, and 46.35 ka.

Despite the muffled signal, the SPC 15 to 30 year^{-1} frequency band contains the same climate insight as WDC. SPC is in agreement with WDC in that there is no correspondence between the 15 to 30 year^{-1} SPC signal and AIM events. The frequency band is responding to a different forcing mechanism and possibly the same mechanism as the frequencies at the WDC site. The two sites also both have spectral peaks of prominence at 32 ka. The SPC signal differs from WDC in that it’s highest power densities are mid 20 ka whereas the 15 to 30 year^{-1} band peaks in the early 30 ka’s. The SPC signal is a lower step at this time but could be artificially low due to diffusion.

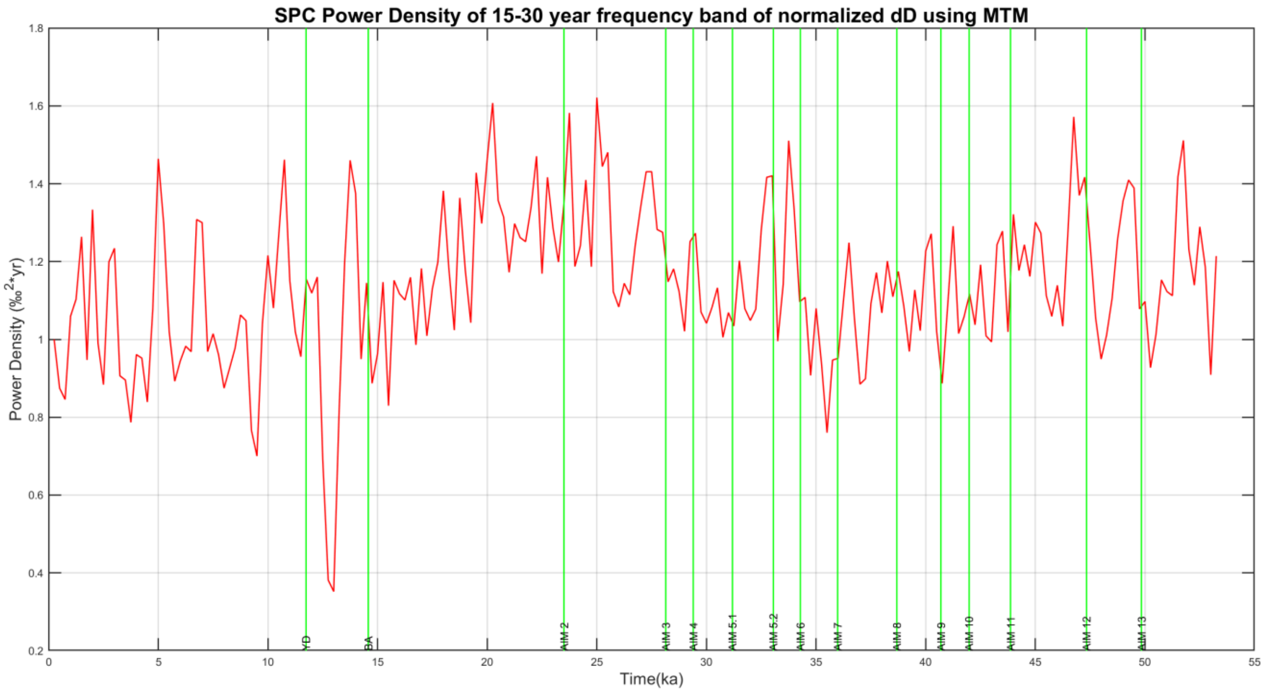

Figure 30: Results of normalized δD MTM spectral analysis of the 15 to 30 year^{-1} frequency band from SPC. The sharp decline in power density around 13 ka is a result of missing data and not representative of actual data. AIM events, the Younger Dryas, and the Bolling-Allerod are plotted as vertical lines on the graph.

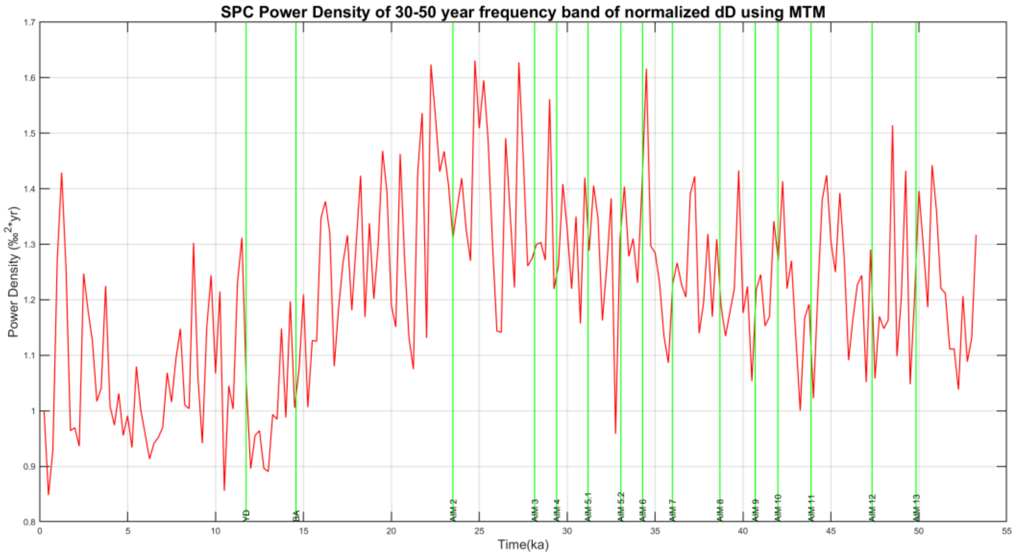

Figure 31: Results of normalized δD MTM spectral analysis of the 30 to 50 year^{-1} frequency band from SPC. AIM events, the Younger Dryas, and the Bolling-Allerod are plotted as vertical lines on the graph.

The 30 to 50 year^{-1} frequency band at SPC is characterized by low power density but high variability in the Holocene, highest spectral power throughout the 20 ka's, and a drop off in spectral power around 31 ka. The signal is comprised of several steps. Step 1 has lower power densities and abnormally high variability for the Holocene. Step 1 lasts from the present to Younger Dryas. There is a regime shift from the Younger Dryas to 16 ka. Step 2 has moderate power density while maintaining high variability and lasts from 16 to 21.5 ka. Step 3 has the highest power density and lasts from 21.5 to 29.5 ka. After Step 3 the power density of the signal decreases through each consecutive step. Step 4 is from 29.5 to 34.75 ka. Step 5 is from 35 to 53.25 ka. There is a large peak at 1.25 ka which could be a result of firn column influence on the data. There are notable spikes at 22.5, 24.75, 27.5, and 34.5 ka. This band does not align with AIM events. The decrease in power density at 31 ka and 16 ka is similar to the 4 to 15 year^{-1} band for WDC. The signal could be a function of ice sheet dynamics as well and could be affected by the size of the Laurentide ice sheet.

4.1.4. Interpretations of dln:

The dln is a hard proxy to interpret, however individual frequencies or frequency bands of dln can be very useful for gathering information about climate. Figures 32 and 33 show a compilation of four different frequency bands through time for both WDC and SPC. The dln was chosen over dxs because dln compensates for super saturation effects near the poles that dxs is impacted by. The trend in spectral power for dln is very similar to δD. The signal is weak for the first 16 ka, strong from 16 to 34 ka, and moderately powerful after that. There is a step-function at 13 ka where the dln decreases towards the present (Figure 32), which is substantially more pronounced than changes seen in δD. The drop may correspond to the Sunda Shelf Flooding of the maritime continent, as mentioned in Jones et al. (2018). The Sunda shelf is a large continental shelf that is currently covered in shallow seas, during periods of lower global sea level the shelf was exposed and covered an area that spanned from Vietnam to the Indonesian archipelago, flooding the shelf would change convection patterns and effect Walker circulation and the ENSO teleconnection system (Hanebuth et al. 2000). During glacial times when the shelf was exposed, the Indo-Pacific warm pool (a key region for warmth and moisture for the globe) was cooler, resulting in changes in atmospheric circulation (Dinezio and Tierney, 2013). Paleo Records show that at the time of the exposure, East Africa got wetter while Indonesia and Australia got drier (Dinezio and Tierney, 2013). In the study by Dinezio and Tierney (2013), the only model to correctly reflect the changes seen in the paleo records was HadCM3 which accomplished this through a weaker Walker circulation over the Indian Ocean that was counterbalanced by stronger Walker circulation in the Pacific Ocean. The flooding of the shelf would, consequently, restore previous Walker circulation patterns. Once flooded, convection would increase over the shelf as the shallow warm water covering the shelf caused more vertical air motion than the previously exposed land did (Dinezio and Tierney, 2013). The change in convection patterns would weaken the Pacific Walker circulation. In West Antarctica, there is a documented connection to Pacific climate patterns (Jones et al. 2018), in that the moisture sources to WDC are in the Pacific. We could expect that dln may be sensitive to these changes since it depends on temperature, humidity, and wind speed at the moisture source. The dln variability would be inherently linked to changes in Walker Circulation in that trade winds would shift with altered convection, as well as sea surface temperatures and humidity.

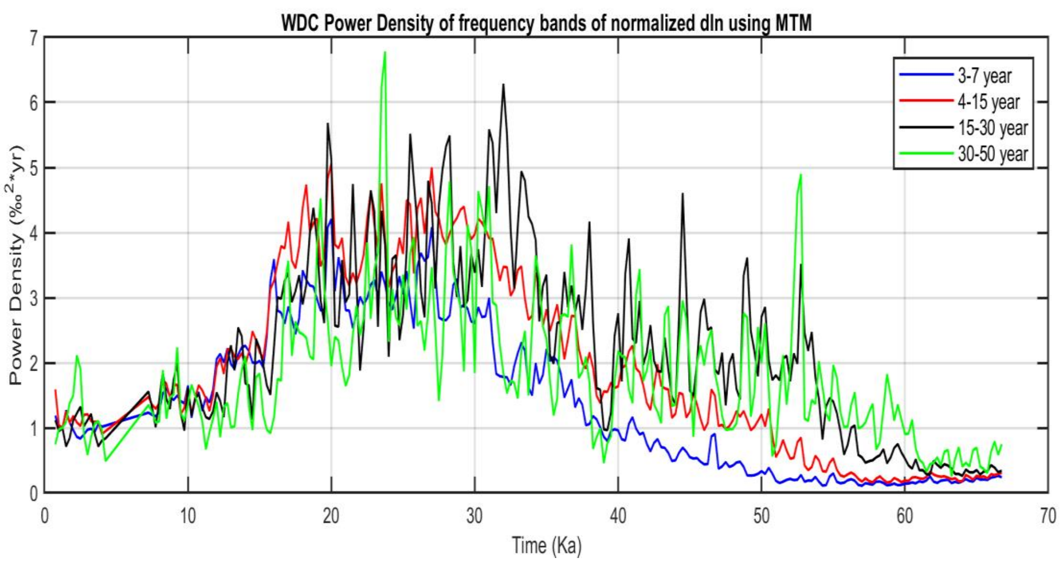

Figure 32: Power Density of the 3-7, 4-15, 15-30, and 30-50 year^{-1} dln bands at WDC using MTM spectral analysis. The data from 4 to 7 ka was deleted because it had data that was not correct.

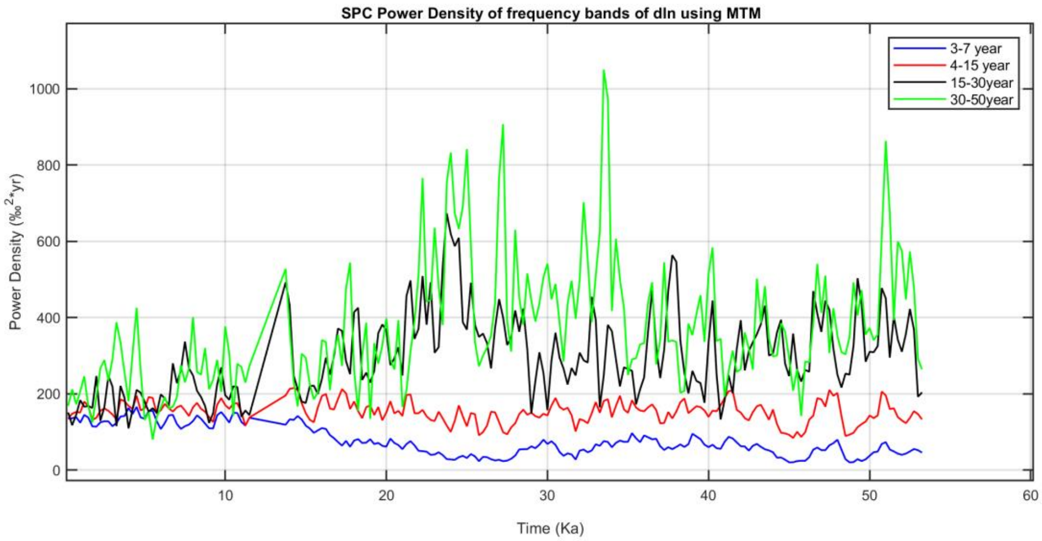

Figure 33: Power Density of the 3-7, 4-15, 15-30, and 30-50 year^{-1} frequency bands of dln at SPC through MTM spectral analysis. The data at around 12 ka was deleted due to the original dataset not containing information at that time.

4.1.5. 20 ka anomaly:

Through analysis of different frequency bands (3-7 yr^{-1}, 4-15 yr^{-1}, 15-30 yr^{-1}, and 30-50 yr^{-1}) at SPC and WDC, there is a clear spike (larger amplitude signals) at ~20 ka that generally occurs in both ice cores at interannual timescales, but not always at decadal timescales. In WDC, the spike appears in 3-7, 4-15, and 30-50 yr^{-1} (Figures 23, 25, 27) while for SPC it occurs in all bands except 30-50 yr^{-1} (Figures 28, 29, 30). The consistency of this peak throughout different frequencies and at both sites suggests a climate anomaly. Larger amplitudes (i.e. the 20 ka spike) could be caused by increased accumulation that reduced the effects of diffusion, or by a change in climate. In WDC and SPC, the 3 to 7 yr^{-1} frequency bands are strongly affected by diffusion. Despite this, the 20 ka spike is seen in both. However, the explanation of increased accumulation and less diffusion is not possible since the WAIS accumulation record shows no increase in accumulation at ~20 ka (Figure 34). Furthermore, the spike is also seen in frequencies that are not affected by diffusion. Thus, the 20 ka spike likely reflects a climate anomaly.

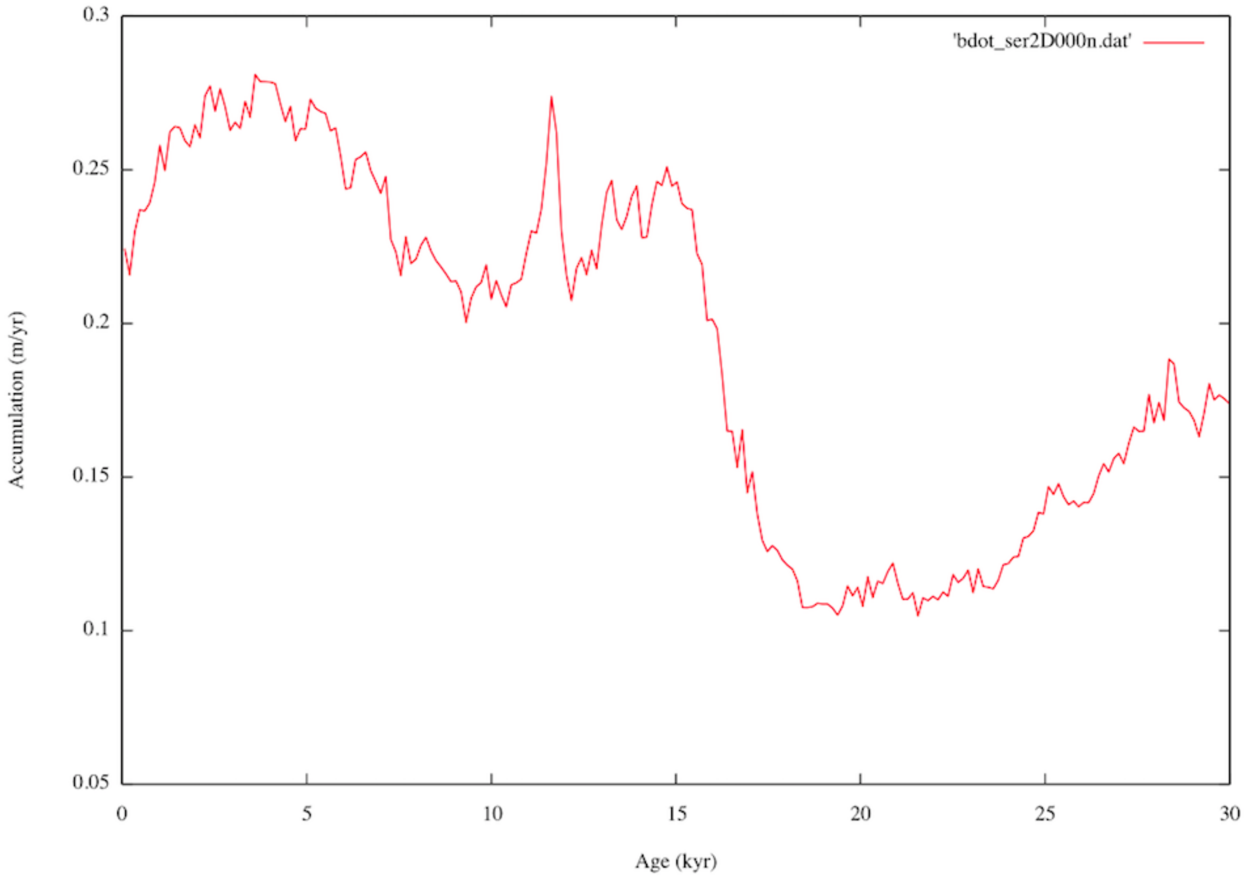

Figure 34: Accumulation record from WDC (Cuffey,2016)

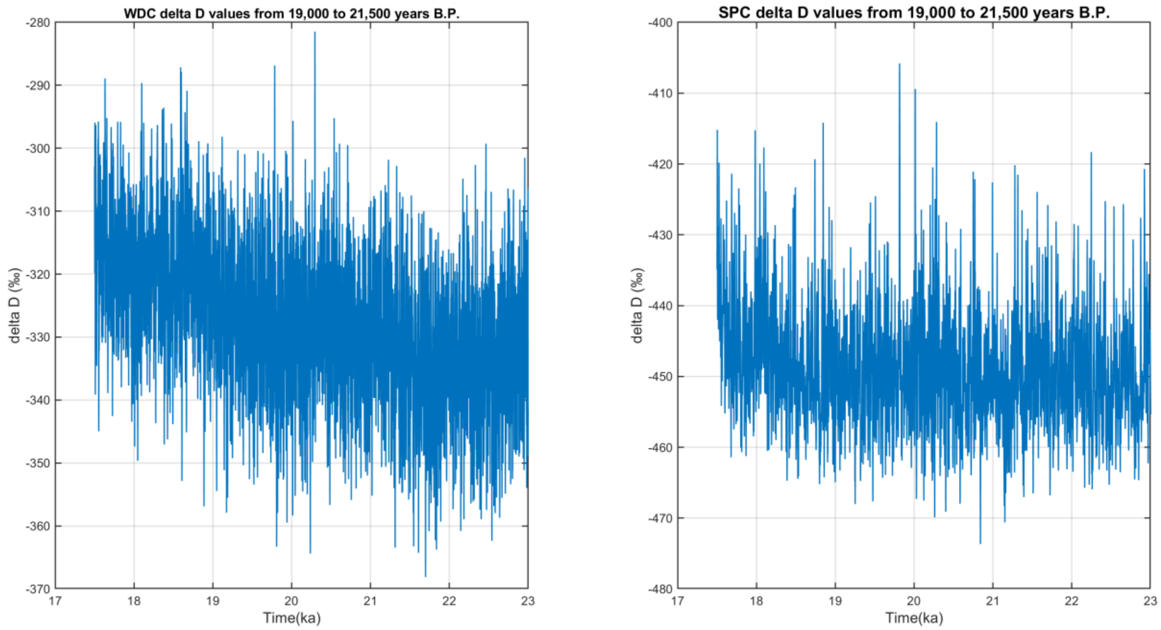

Figure 35: Plot of δD from 19 ka to 21.5 ka for WDC and SPC. While not evident in the direct plots of water isotopes vs. time, spectral analysis suggests climate oscillations at interannual timescales at 20 ka that are not typical compared to the surrounding time periods.

The WAIS Divide Project members (2013) identified the beginning of the deglaciation as a regime shift at 20 ka in water isotope and sea salt sodium (ssNa) records. As a proxy, ssNa is debated as reflecting either a decrease in sea ice extent or the strength of atmospheric circulation. The inverse relationship between ssNa and water isotope values were interpreted as changes in sea ice extent and not atmospheric circulation (WAIS Divide Project Members, 2013). The change in sea ice aligned with an increasing trend in local insolation values. The WAIS Divide Project Members (2013) found that interior Antarctic cores were not affected by insolation and sea ice changes. No such analysis was done for SPC, which was drill two years after WDC.

The presence of increased interannual and decadal variability at SPC at 20 ka suggests that the continental interior was impacted by the climate regime shift. How the results of the WAIS Divide Project Members (2013) and our results are linked is unclear, except that we now have evidence that the changes occurring to the climate system were expressed at high-frequencies, including the 3-7 yr^{-1} band. It is possible that we are observing a type of critical slowdown. Critical slowdown theory hypothesizes that before a major change in the equilibrium state of a system there are signs of the coming change (Lenton et al., 2012). In water isotope space, these precursor signs would be expressed as increased variance in data and low recovery from perturbations (Lenton et al. 2012; Figure 36). We see increased variability at ~20 ka in the form of amplitude increases in interannual and decadal frequency bands. These results suggest that high frequency amplitude increases are an indicator, a precursor, or at least linked in some way, to substantial climate transitions.

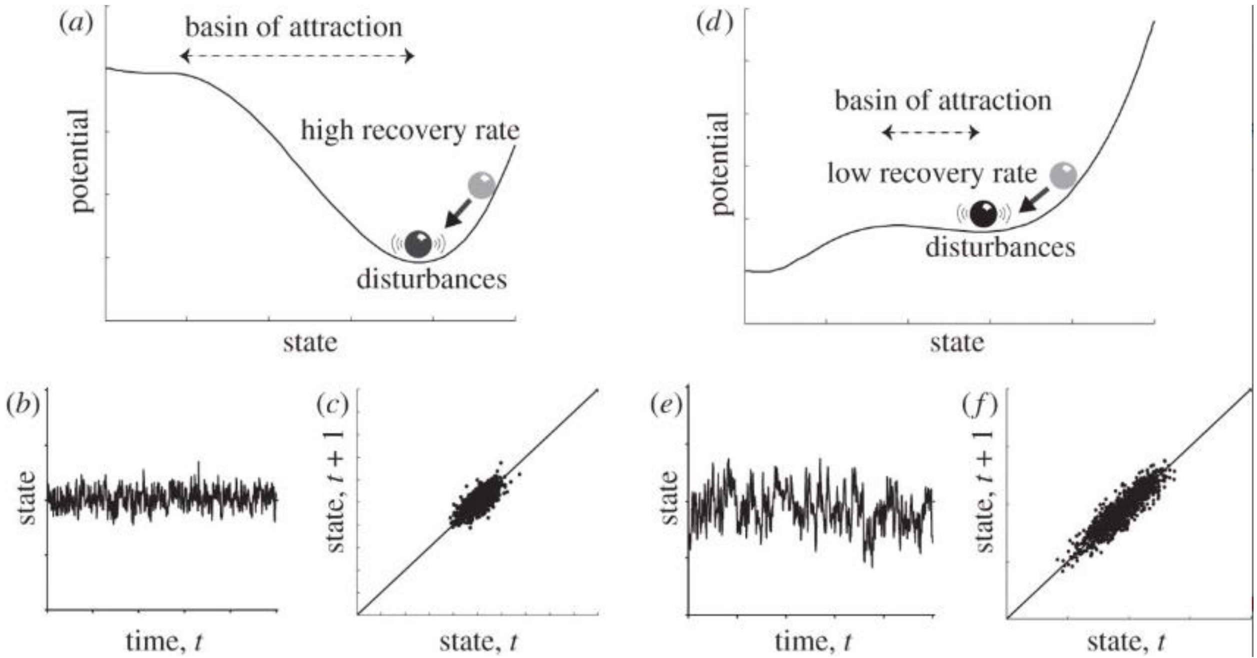

Figure 36: a,b, and c show a stable background climate state. D, e, and f show a climate system as it is transitioning to a new climate regime. Transitions are characterized by high variance in data and low recovery from perturbations (Lenton et al. 2012).

Section 5: Conclusion

Spectral analysis is an essential tool for paleoclimate record analysis, the technique builds upon information seen in isotope space by giving insight into the climate cycles that determine isotope values. With spectral analysis it is possible to determine how frequency bands change in strength over time and potentially see precursors to climate change through amplitude increases of frequencies before a climate regime shift.

This study found that AIM events were not correlated with high frequency signals suggesting that AIM events are a function of long term, millennial scale, climate cycles and not simply a short lived shift in the climate state to a high frequency controlled system. This observation could provide insight into the AMOC system, the bipolar seesaw, and the cause of AIM and D-O events. Investigation of high frequency signals in high-resolution Greenland cores should be pursued in future studies. If high-resolution Greenland cores, such as EGRIP, found a similar discordance between D-O events and high frequency signals, there could be a fundamental change in the understanding of the bipolar seesaw. Similar analysis of other high-resolution records could confirm the presence of spectral spikes seen in the records such as the 34.5 ka peak seen in the WDC and SPC 30-50 year^{-1} frequency band.

The study also tested the use of plotting individual frequencies and their power density through time as a means of interpreting the basic role of diffusion in lowering power densities. This preliminary separation method allowed for heavily impacted diffusion signals to be recognized. Although not exact, this method could be utilized in future studies to determine how necessary diffusion corrections are for research in individual frequency bands contained in proxy records. Out of the sources of diffusion (firn, solid ice, geothermal, and CFA) only modeling for firn and CFA diffusion corrections have been effective at correcting the impact of diffusion on the water isotope record. We did not undertake a diffusion correction in this study. In future studies, our results could be improved through a full diffusion analysis.

The analysis of SPC and WDC allowed for spectral and spatial correspondence to be reached for some interpretations. Although muffled, the SPC in general mirrored trends and events seen in the WDC frequencies. Spatial agreement across spectral bands help prove the global significance of the events and trends seen throughout the WDC record. The results of the 4 to 15 year^{-1} band provide support to (Jones et al, 2018) on their analysis of the decline of power density of the band at 16 ka and overall trends in the data corresponding to the Laurentide ice sheet size. This study found the same decline and general trend in the strength of the 4 to 15 year^{-1} band as the ones found in the 2018 study. Analysis could be improved in future studies through the incorporation of global circulation models. These models would help extrapolate the results to a wider region and help differentiate the influence of different oceans on the signal such as how much WDC and SPC communicated with the Pacific in comparison to other ocean basins.

Spectral and spatial coverage lead to the discovery of a potential increase in amplitude for high frequencies in response to a critical slowdown. This event was observed at 20 ka across both sites as a spike in power density. The WAIS Divide Project Members (2013) noted this event as changes in sea ice extent 2,000 years before significant warming in other parts of Antarctica and showed this time period marked the beginning of the deglaciation. If correct, spectral analysis could be a different lense for viewing critical slowdowns. Analysis of other high-resolution cores throughout Antarctica or more analyzed frequency bands could be utilized in the future to find the extent and amplitude of the 20 ka spatially and spectrally in other regions of Antarctica.

In this study, a decrease in dln strength at 13 ka was suggested to connect to the flooding of the Sunda Shelf and potential changes in Walker circulation and the ENSO teleconnection. To increase the certainty of this interpretation, dln analysis techniques and diffusion correction need to be improved. Since δD and δ^{18}O diffuse at different rates in the firn, it can create a non-climate induced annual signal (Johnsen et al. 2000) that can make climate interpretations difficult. Future studies into dln analysis and efforts to reduce the impact of diffusion would also provide significance and interpretations to other time periods in the analysis.

References:

Adolphi, F., Muscheler, R., Svensson, A., Aldahan, A., Possnert, G., Beer, J., … Thiéblemont, R. (2014). Persistent link between solar activity and Greenland climate during the Last Glacial Maximum. Natur

Andersen, K. K., Azuma, N., Barnola, J. M., Bigler, M., Biscaye, P., Caillon, N., … White, J. W. C. (2004). High-resolution record of Northern Hemisphere climate extending into the last interglacial period.

April S. Dalton Sarah A. Finkelstein Steven L. Forman Peter J. Barnett Tamara Pico Jerry X. Mitrovica. (2019). Was the Laurentide Ice Sheet significantly reduced during Marine Isotope Stage 3? Geology, 47(2), 111–114.

Benetti, M., Reverdin, G., Pierre, C., Merlivat, L., Risi, C., Steen-Larsen, H. C., & Vimeux, F. (2014). Deuterium excess in marine water vapor: Dependency on relative humidity and surface wind speed dur

Blunier, T., & Brook, E. J. (2001). Timing of millennial-scale climate change in antarctica and greenland during the last glacial period. Science. https://doi.org/10.1126/science.291.5501.109

Broecker, W. S. (1998). Paleocean circulation during the last deglaciation: A bipolar seesaw? Paleoceanography. https://doi.org/10.1029/97PA03707

Buizert, C., Cuffey, K. M., Severinghaus, J. P., Baggenstos, D., Fudge, T. J., Steig, E. J., … Taylor, K. C. (2015). The WAIS Divide deep ice core WD2014 chronology – Part 1: Methane synchronizatio

Buizert, C., & Schmittner, A. (2015). Southern Ocean control of glacial AMOC stability and Dansgaard-Oeschger interstadial duration. Paleoceanography. https://doi.org/10.1002/2015PA002795

Casado, M., Landais, A., Picard, G., Münch, T., Laepple, T., Stenni, B., … Jouzel, J. (2018). Archival processes of the water stable isotope signal in East Antarctic ice cores. Cryosphere. https://doi

Craig, H., & Gordon, L. I. (1965). Stable isotopes in oceanographic studies and Paleotemperatures. International Workshop on the Isotopic Effects in Evaporation Revisiting the Craig-Gordon Model Four

Craig, H., Gordon, L. I., & Horibe, Y. (2012). Isotopic exchange effects in the evaporation of water: 1. Low-temperature experimental results. Journal of Geophysical Research. https://doi.org/10.1

Crosson, E. R. (2008). A cavity ring-down analyzer for measuring atmospheric levels of methane, carbon dioxide, and water vapor. In Applied Physics B: Lasers and Optics. https://doi.org/10.1007/s00340

Cuffey, K. M., Clow, G. D., Steig, E. J., Buizert, C., Fudge, T. J., Koutnik, M., … Severinghaus, J. P. (2016). Deglacial temperature history of West Antarctica. Proceedings of the National Academy of Sciences. https://doi.org/10.1073/pnas.1609132113

Dansgaard, W. (2012). Stable isotopes in precipitation. Tellus. https://doi.org/10.3402/tellusa.v16i4.8993

Dinezio, P. N., & Tierney, J. E. (2013). The effect of sea level on glacial Indo-Pacific climate. Nature Geoscience. https://doi.org/10.1038/ngeo1823

Dütsch, M., Pfahl, S., & Sodemann, H. (2017). The impact of nonequilibrium and equilibrium fractionation on two different deuterium excess definitions. Journal of Geophysical Research: Atmospheres

Epstein, S., Buchsbaum, R., Lowenstam, H. a, & Urey, H. C. (1953). Revised Carbonate-Water Isotopic Temeprature Scale. Geological Society of America Bulletin. https://doi.org/10.1130/0016-7606(195

Fisher, A. T., Mankoff, K. D., Tulaczyk, S. M., Tyler, S. W., & Foley, N. (2015). High geothermal heat flux measured below the West Antarctic Ice Sheet. Science Advances. https://doi.org/10.1126/sciadv.1500093

Fisher, D. A., Reeh, N., & Clausen, H. B. (2017). Stratigraphic Noise in Time Series Derived from Ice Cores. Annals of Glaciology. https://doi.org/10.1017/s0260305500005942

Galewsky, J., Steen-Larsen, H. C., Field, R. D., Worden, J., Risi, C., & Schneider, M. (2016). Stable isotopes in atmospheric water vapor and applications to the hydrologic cycle. Reviews of Geophysic

Gat, J. R. (2002). OXYGEN AND HYDROGEN ISOTOPES IN THE HYDROLOGIC CYCLE. Annual Review of Earth and Planetary Sciences. https://doi.org/10.1146/annurev.earth.24.1.225

Hanebuth, T., Stattegger, K., & Grootes, P. M. (2000). Rapid flooding of the Sunda Shelf: A late-glacial sea-level record. Science. https://doi.org/10.1126/science.288.5468.1033

Jeyaseelan, A. S., & Balaji, R. (2015). Spectral analysis of wave elevation time histories using multi-taper method. Ocean Engineering. https://doi.org/10.1016/j.oceaneng.2015.06.051

Jones, T. R., Roberts, W. H. G., Steig, E. J., Cuffey, K. M., Markle, B. R., & White, J. W. C. (2018). Southern Hemisphere climate variability forced by Northern Hemisphere ice-sheet topography. Nature. https://doi.org/10.1038/nature24669

Kaufmann, P. R., Federer, U., Hutterli, M. A., Bigler, M., Schüpbach, S., Ruth, U., … Stocker, T. F. (2008). An improved continuous flow analysis system for high-resolution field measurements on ice cores. Environmental Science and Technology. https://doi.org/10.1021/es8007722

Labeyrie, L., Skinner, L., & Cortijo, E. (2013). PALEOCLIMATE RECONSTRUCTION | Sub-Milankovitch (DO/Heinrich) Events. In Encyclopedia of Quaternary Science. https://doi.org/10.1016/b978-0-444-53643-3.00014-5

Lenton, T. M., Livina, V. N., Dakos, V., Van Nes, E. H., & Scheffer, M. (2012). Early warning of climate tipping points from critical slowing down: Comparing methods to improve robustness. Philosophical Transactions of the Royal Society A: Mathematical, Physical and Engineering Sciences. https://doi.org/10.1098/rsta.2011.0304

Lewis, S. C., Legrande, A. N., Kelley, M., & Schmidt, G. A. (2013). Modeling insights into deuterium excess as an indicator of water vapor source conditions. Journal of Geophysical Research Atmospheres. https://doi.org/10.1029/2012JD017804

Lisiecki, L. E. (2010). Links between eccentricity forcing and the 100,000-year glacial cycle. Nature Geoscience. https://doi.org/10.1038/ngeo828

Lisiecki, L. E., & Raymo, M. E. (2005). A Pliocene-Pleistocene stack of 57 globally distributed benthic δ 18O records. Paleoceanography. https://doi.org/10.1029/2004PA001071

Luz, B., Barkan, E., Yam, R., & Shemesh, A. (2009). Fractionation of oxygen and hydrogen isotopes in evaporating water. Geochimica et Cosmochimica Acta. https://doi.org/10.1016/j.gca.2009.08.008

Masson-Delmotte, V., Hou, S., Ekaykin, A., Jouzel, J., Aristarain, A., Bernardo, R. T., … White, J. W. C. (2008). A review of antarctic surface snow isotopic composition: Observations, atmospheric circulation, and isotopic modeling. Journal of Climate. https://doi.org/10.1175/2007JCLI2139.1

McPhaden, M. J., Zebiak, S. E., & Glantz, M. H. (2006). ENSO as an integrating concept in earth science. Science. https://doi.org/10.1126/science.1132588

Okitsugu Watanabe, Hitoshi Shoji, Kazuhide Satow, Hideaki Motoyama, Yoshiyuki Fujii, Hideki Narita, S. A. and 仁 庄子. (2003). Dating of the Dome Fuji, Antarctica deep ice core. National Institute of Polar Research.

Parrenin, F., Barnola, J. M., Beer, J., Blunier, T., Castellano, E., Chappellaz, J., … Wolff, E. (2007). The EDC3 chronology for the EPICA Dome C ice core. Climate of the Past. https://doi.org/10.5194/cp-3-485-2007

Percival, D. B., & Walden, A. T. (2009). Spectral Analysis for Physical Applications. Spectral Analysis for Physical Applications. https://doi.org/10.1017/cbo9780511622762

Pfahl, S., & Sodemann, H. (2014). What controls deuterium excess in global precipitation? Climate of the Past. https://doi.org/10.5194/cp-10-771-2014

Rasmussen, T. L., Thomsen, E., & Moros, M. (2016). North Atlantic warming during Dansgaard-Oeschger events synchronous with Antarctic warming and out-of-phase with Greenland climate. Scientific Reports. https://doi.org/10.1038/srep20535

Schoenemann, S. W., Steig, E. J., Ding, Q., Markle, B. R., & Schauer, A. J. (2014). Triple water-isotopologue record from WAIS Divide, Antarctica: Controls on glacial-interglacial changes in 17Oexcess of precipitation. Journal of Geophysical Research. https://doi.org/10.1002/2014JD021770
Schulz, M. (2002). On the 1470-year pacing of Dansgaard-Oeschger warm events. Paleoceanography. https://doi.org/10.1029/2000pa000571

Schwander, J., & Stauffer, B. (1984). Age difference between polar ice and the air trapped in its bubbles. Nature. https://doi.org/10.1038/311045a0

Sigl, M., Fudge, T. J., Winstrup, M., Cole-Dai, J., Ferris, D., McConnell, J. R., … Sowers, T. A. (2016). The WAIS Divide deep ice core WD2014 chronology - Part 2: Annual-layer counting (0-31 ka BP). Climate of the Past. https://doi.org/10.5194/cp-12-769-2016

Steen-Larsen, H. C., Johnsen, S. J., Masson-Delmotte, V., Stenni, B., Risi, C., Sodemann, H., … White, J. W. C. (2013). Continuous monitoring of summer surface water vapor isotopic composition above the Greenland Ice Sheet. Atmospheric Chemistry and Physics. https://doi.org/10.5194/acp-13-4815-2013

Steen-Larsen, H. C., Masson-Delmotte, V., Hirabayashi, M., Winkler, R., Satow, K., Prié, F., … Sveinbjörnsdottír, A. E. (2014). What controls the isotopic composition of Greenland surface snow? Climate of the Past. https://doi.org/10.5194/cp-10-377-2014

Steen-Larsen, H. C., Masson-Delmotte, V., Sjolte, J., Johnsen, S. J., Vinther, B. M., Bréon, F. M., … White, J. (2011). Understanding the climatic signal in the water stable isotope records from the NEEM shallow firn/ice cores in northwest Greenland. Journal of Geophysical Research Atmospheres.

Trenberth, K. E. (1997). The Definition of El Niño. Bulletin of the American Meteorological Society. https://doi.org/10.1175/1520-0477(1997)078<2771:TDOENO>2.0.CO;2

Uemura, R., Matsui, Y., Yoshimura, K., Motoyama, H., & Yoshida, N. (2008). Evidence of deuterium excess in water vapor as an indicator of ocean surface conditions. Journal of Geophysical Research Atmospheres. https://doi.org/10.1029/2008JD010209

Ullman, D. J., Legrande, A. N., Carlson, A. E., Anslow, F. S., & Licciardi, J. M. (2014). Assessing the impact of laurentide ice sheet topography on glacial climate. Climate of the Past. https://doi.org/10.5194/cp-10-487-2014

WAIS Divide Project Members, Fudge, T. J., Steig, E. J., Markle, B. R., Schoenemann, S. W., Ding, Q., … Wong, G. J. (2013). Onset of deglacial warming in West Antarctica driven by local orbital forcing. Nature. https://doi.org/10.1038/nature12376

Wunsch, C. (2003). The spectral description of climate change including the 100 ky energy. Climate Dynamics. https://doi.org/10.1007/s00382-002-0279-z

WAIS, Buizert, C., Adrian, B., Ahn, J., Albert, M., Alley, R. B., … Woodruff, T. E. (2015). Precise interpolar phasing of abrupt climate change during the last ice age. Nature. https://doi.org/10.1038/nature14401